

Cell-Type-Resolved Neuromodulator Receptor Expression in the Basolateral Amygdala and Medial Prefrontal Cortex: A Multi-Modal Transcriptomic Atlas for Psychedelic and Anxiolytic Drug Targets

Abstract

The basolateral amygdala (BLA) and medial prefrontal cortex (mPFC) form a reciprocal circuit central to threat processing, fear learning, and the pathophysiology of anxiety disorders. Monoaminergic neurotransmitter systems—serotonin, norepinephrine, and dopamine—powerfully modulate this circuit, yet comprehensive cell-type-resolved maps of receptor expression have been lacking. Here we systematically characterize the expression of 28 neuromodulator receptor genes across all major neuronal and glial cell types in the mouse BLA and mPFC using two complementary platforms from the Allen Brain Cell Atlas: 10x single-nucleus RNA sequencing (snRNA-seq; 28,809 BLA neurons, 165,539 mPFC neurons, plus glia) and MERFISH spatial transcriptomics (8,238 BLA cells, 64,474 mPFC cells; 11 shared receptor genes). We reveal striking cell-type specificity for psychedelic-relevant serotonin receptors: Htr2a is highest in parvalbumin and Lamp5 interneurons in BLA and in deep-layer excitatory neurons in mPFC; Htr2c shows dramatic enrichment in Sncg interneurons, L5 near-projecting neurons, and BLA excitatory populations; Htr1a is concentrated in Sst Chodl and chandelier interneurons; and Htr7 is enriched in deep-layer corticothalamic neurons and chandelier cells. Noradrenergic receptors display complementary patterns, with Adrb1 dominant in excitatory neurons and Adra1a/Adra1b preferentially targeting interneuron subtypes. Cross-modality validation demonstrates strong agreement between platforms (Spearman rho = 0.79-0.88), establishing high-confidence consensus rankings for experimental prioritization. Cross-region comparison reveals largely conserved interneuron receptor profiles (rho = 0.94) but significant regional differences, including BLA enrichment of Htr2c (log₂ fold-change +1.6) and Adra2a (+1.1), and mPFC enrichment of Adra1b (-1.2). MERFISH spatial analysis further resolves expression gradients across BLA substructures (BLAa, BLAp, BLAv) and mPFC areas (PL, ILA, ACAd, ACAv). These findings provide a molecular foundation for understanding how psychedelics, anxiolytics, and other monoaminergic drugs differentially engage specific cell populations within fear and anxiety circuits, with direct implications for the development of more selective therapeutics.

1. Introduction

The reciprocal circuitry connecting the basolateral amygdala (BLA) and medial prefrontal cortex (mPFC) forms a central substrate for threat processing, fear learning, and the pathophysiology of anxiety disorders. The BLA functions as a primary site for encoding the valence and salience of threat-related stimuli, integrating sensory information with contextual cues to drive both adaptive and maladaptive fear responses. The mPFC

exerts top-down regulatory control over these responses through anatomically and functionally distinct subdivisions: the prelimbic cortex (PL) facilitates fear expression and maintains conditioned fear responses, the infralimbic cortex (IL) promotes fear extinction and safety learning, and the dorsal anterior cingulate cortex (dACC) mediates conflict monitoring and behavioral adaptation under threat uncertainty. Disruption of BLA-mPFC connectivity is strongly implicated in anxiety disorders, post-traumatic stress disorder (PTSD), and pathological fear states that resist extinction. Understanding the molecular mechanisms that modulate activity within and between these structures is therefore critical for developing more effective treatments for stress-related psychiatric conditions.

Monoaminergic neurotransmitter systems—serotonin, norepinephrine, and dopamine—exert powerful modulatory influences over BLA-mPFC circuit dynamics. Serotonergic projections from the dorsal and median raphe nuclei innervate both structures densely, regulating excitability, synaptic plasticity, and behavioral responses to threat through a complex array of receptor subtypes. Noradrenergic inputs from the locus coeruleus similarly modulate arousal, attention to threat-related cues, and the encoding and consolidation of fear memories. Dopaminergic projections from the ventral tegmental area contribute to reward-related learning and motivational valence, but also play important roles in fear conditioning and extinction processes. Dysregulation of monoaminergic signaling is a common feature across anxiety disorders, major depression, and PTSD, and the vast majority of pharmacological treatments for these conditions target monoamine receptors or transporters. Despite decades of research establishing the importance of monoaminergic modulation in fear and anxiety circuits, we lack comprehensive, cell-type-resolved maps of receptor expression that could explain the diverse and sometimes contradictory effects of drugs targeting these systems.

Of particular current interest are the receptors engaged by classical psychedelic compounds, which have emerged as promising therapeutic agents for treatment-resistant depression, PTSD, and anxiety disorders. Psychedelics such as psilocybin, LSD, and DMT exert their primary effects through agonism at serotonin 2A receptors (encoded by the *Htr2a* gene), and the density of cortical 5-HT2A receptors correlates with psychedelic potency and subjective effects. However, 5-HT2A receptor activation does not occur in isolation. The therapeutic and subjective effects of psychedelics are strongly modulated by other serotonin receptor subtypes that are co-expressed in overlapping and distinct cell populations. The serotonin 1A receptor (*Htr1a*) has well-established anxiolytic properties and is the target of the partial agonist buspirone; 5-HT1A activation can attenuate certain psychedelic effects, and polymorphisms in this receptor are associated with individual differences in psychedelic response. The serotonin 2C receptor (*Htr2c*) often opposes the effects of 5-HT2A signaling and has been implicated in anxiety, obsessive-compulsive disorder, and the side effect profiles of serotonergic drugs; notably, 5-HT2C inverse agonism may contribute to the antidepressant effects of several atypical antipsychotics. The serotonin 7 receptor (*Htr7*), while less studied, has emerged as a novel target for fear extinction facilitation and rapid antidepressant effects in preclinical models. Understanding which specific cell types in fear and anxiety circuits express these receptors—and in what relative abundance—is essential for predicting how psychedelics and related compounds modulate circuit function, for understanding why these

drugs produce therapeutic benefits in some individuals but adverse reactions in others, and for developing the next generation of more selective and targeted psychedelic-inspired therapies.

The noradrenergic system similarly presents a complex receptor landscape with clear therapeutic relevance. The locus coeruleus-norepinephrine system is the brain's primary arousal and stress response network, and hyperactivity of this system is a cardinal feature of anxiety disorders and PTSD. Alpha-2 adrenergic receptors (*Adra2a*, *Adra2c*) function primarily as autoreceptors and inhibitory modulators; alpha-2 agonists such as clonidine and guanfacine are used clinically to reduce hyperarousal, improve executive function in ADHD, and treat PTSD symptoms. Alpha-1 receptors (*Adra1a*, *Adra1b*, *Adra1d*) mediate excitatory noradrenergic signaling, and the alpha-1 antagonist prazosin is widely prescribed for PTSD-related nightmares and sleep disturbances, though its efficacy remains debated. Beta-adrenergic receptors (*Adrb1*, *Adrb2*, *Adrb3*) are critically involved in the formation and reconsolidation of emotional memories; the beta-blocker propranolol has been investigated extensively as a tool to disrupt fear memory reconsolidation when administered during memory reactivation. The opposing effects of alpha-1 blockade versus alpha-2 agonism, and the memory-specific effects of beta-blockade, suggest that these receptor subtypes are differentially distributed across cell types within fear circuits, but comprehensive cell-type-resolved expression data have been lacking.

Dopamine receptors also contribute to BLA-mPFC circuit function, though they have received less emphasis in the anxiety and psychedelic literature. D1-like receptors (*Drd1*, *Drd5*) and D2-like receptors (*Drd2*, *Drd3*, *Drd4*) in both the BLA and mPFC modulate fear conditioning, extinction, and the flexible updating of threat representations. Dopaminergic signaling in the mPFC is particularly important for working memory and cognitive control functions that support behavioral adaptation under uncertainty.

Despite this extensive pharmacological and behavioral literature, fundamental gaps remain in our understanding of the cellular architecture underlying monoaminergic modulation of fear and anxiety circuits. Most studies have relied on bulk tissue measurements, autoradiographic receptor binding, or *in situ* hybridization approaches that provide anatomical resolution but lack information about the specific cell types expressing each receptor. We know that pyramidal neurons and GABAergic interneurons have fundamentally different roles in circuit computation, and that interneuron subtypes—including parvalbumin-expressing (*Pvalb*), somatostatin-expressing (*Sst*), vasoactive intestinal peptide-expressing (*Vip*), and *Lamp5*-expressing populations—exert distinct forms of inhibitory control. Without knowing which of these cell types express which receptors, and at what levels, we cannot fully predict how systemic drug administration will alter circuit function or why different individuals show different responses to the same compound.

The Allen Brain Cell Atlas for the whole mouse brain now provides an unprecedented resource to address these questions. This dataset comprises single-nucleus RNA-sequencing data from over four million cells across the entire brain, combined with spatially-resolved MERFISH transcriptomic data that maintains anatomical context. The taxonomic resolution distinguishes over 5,000 distinct cell types, including detailed characterization of excitatory projection neuron subtypes defined by layer and projection target, as well as molecularly defined interneuron subtypes. In the present study, we systematically characterize the expression of

28 monoaminergic receptor genes across all major neuronal cell types in the BLA and mPFC using both 10x single-nucleus RNA-sequencing and MERFISH spatial transcriptomics. We compare receptor expression profiles across these two platforms to validate cell-type-specific patterns, examine similarities and differences between BLA and mPFC, assess whether receptor expression varies across anatomical subdivisions within each region, and establish consensus cell-type rankings that identify which populations are most likely to be directly modulated by specific receptor-targeted drugs. This comprehensive cell-type-resolved receptor atlas provides a molecular foundation for understanding monoaminergic modulation of fear and anxiety circuits and for predicting the cellular targets of psychedelic and anxiolytic therapeutics.

2. Methods

2.1 Data Source

All analyses used the Allen Brain Cell Atlas release 20251031, accessed via the `AbcProjectCache` API from the `abc_atlas_access` Python package. The Whole Mouse Brain (WMB) dataset comprises 4,042,976 cells profiled by 10x Chromium single-nucleus RNA sequencing (snRNA-seq) spanning 32,285 genes, and 4,334,174 cells profiled by multiplexed error-robust fluorescence in situ hybridization (MERFISH) spanning a targeted 550-gene panel. Data were downloaded from AWS S3 using `AbcProjectCache.from_s3_cache()` and cached locally for subsequent analyses.

2.2 Cell Type Taxonomy

Cell type annotations followed the WMB-taxonomy hierarchical classification system with five levels: neurotransmitter, class, subclass, supertype, and cluster. Taxonomy annotations were joined to cell metadata using the `cluster_to_cluster_annotation_membership_pivoted` table, which maps each `cluster_alias` to all annotation levels. This enabled flexible aggregation at subclass (12 major cell types in BLA, 20 in mPFC) or supertype (68 finer subtypes in BLA, 101 in mPFC) resolution.

2.3 Brain Region Definitions

For 10x data, brain regions were defined by dissection-based region-of-interest labels. BLA cells were identified within the cortical subplate (CTXsp) dissection region by filtering to BLA-specific excitatory neuron subclasses (LA-BLA-BMA-PA Glut, MEA-COA-BMA Ccdc42 Glut) plus major cortical GABAergic interneuron subclasses (Pvalb, Sst, Vip, Lamp5, Sncg subtypes). This approach yielded 28,809 neuronal cells; an additional 25,304 glial cells (Astro-TE, Microglia) from CTXsp were included for complete cellular profiling. mPFC cells were extracted from the PL-ILA-ORB (prelimbic, infralimbic, orbital areas; 106,044 cells) and ACA (anterior cingulate; 102,825 cells) dissection regions, filtered to excitatory layer types (L2/3 IT, L5 IT, L5 ET, L6 IT, L6 CT, L6b) and interneurons, yielding 172,362 neuronal cells plus 14,917 glia. A critical limitation is that 10x interneurons in CTXsp are dissection-region-wide and not exclusively BLA-localized.

For MERFISH data, spatial registration to the Allen Common Coordinate Framework (CCF) enabled precise anatomical parcellation. BLA cells were identified by `parcellation_structure == 'BLA'`, yielding 13,233 cells across three substructures: BLAa (anterior, 5,933 cells), BLAp (posterior, 4,647 cells), and BLAv (ventral, 2,653 cells). mPFC cells were defined by parcellation to PL, ILA, ACAd (dorsal), and ACAv (ventral), totaling 64,474 cells. All MERFISH cell types, including interneurons and glia, are spatially confirmed within their assigned brain structures.

2.4 Neuromodulator Receptor Gene Selection

We analyzed 28 neuromodulator receptor genes: 14 serotonin receptors (Htr1a, Htr1b, Htr1d, Htr1f, Htr2a, Htr2b, Htr2c, Htr3a, Htr3b, Htr4, Htr5a, Htr5b, Htr6, Htr7), 9 norepinephrine (adrenergic) receptors (Adra1a, Adra1b, Adra1d, Adra2a, Adra2b, Adra2c, Adrb1, Adrb2, Adrb3), and 5 dopamine receptors (Drd1, Drd2, Drd3, Drd4, Drd5). All 28 genes were present in the 10x transcriptome. Of these, 11 genes (Htr1b, Htr1d, Htr2a, Htr3a, Htr7, Adra1a, Adra1b, Drd1, Drd2, Drd3, Drd5) were included in the MERFISH 550-gene panel and used for cross-modality comparisons.

2.5 Expression Data Extraction

For 10x data, log2-normalized expression matrices were accessed as backed AnnData objects (.h5ad format) using `anndata.read_h5ad(backed='r')`. Expression matrices are organized by chemistry (10Xv2, 10Xv3) and dissection region. For each region, cells were subset by boolean indexing converted to integer arrays via `np.where()` to avoid issues with backed array chaining. Gene subsets were extracted similarly, and resulting data were loaded into memory via `.to_memory()` before conversion to pandas DataFrames. Expression values for each (cell x gene) combination were cached to CSV files for rapid reloading.

For MERFISH data, the expression matrix (C57BL6J-638850/log2, 7.6 GB) was accessed as a backed AnnData object. The 11 receptor genes were extracted for cells matching CCF parcellation criteria using the same integer indexing approach as 10x, loaded to memory, and cached to CSV.

2.6 Dot Plot Visualization

Receptor expression patterns were visualized using scanpy's `sc.pl.dotplot()` function. Dot plots display mean expression (color intensity) and fraction of expressing cells (dot size) for each gene-by-cell-type combination. Gene expression was variance-normalized (`standard_scale='var'`) to enable cross-gene comparisons. Genes were grouped by neuromodulator family (serotonin, norepinephrine, dopamine) on the x-axis, with cell types (subclass or supertype level) on the y-axis. Dot plots were generated separately for BLA and mPFC, each at both subclass (coarse) and supertype (fine) resolutions, and with glia included for comprehensive cellular profiling.

2.7 Cross-Modality Analysis

To compare 10x and MERFISH expression profiles, per-subclass mean expression and fraction expressing were computed for the 11 shared receptor genes across shared cell types (10 in BLA: 2 excitatory, 8 interneuron/glia; 18 in mPFC: 9 excitatory, 9 interneuron/glia). Overall agreement was assessed via Pearson and Spearman correlations for all (gene x cell type) combinations. Per-gene correlations evaluated whether each receptor's cell-type specificity was consistent between modalities. Per-cell-type correlations assessed whether each subclass's receptor profile was reproducible. Cell types were ranked by fraction expressing for each gene in each modality, and rank differences quantified cross-platform agreement. Consensus rankings were computed as the average of 10x and MERFISH ranks, with confidence scores defined as $1 - (|\text{rank difference}| / \text{max possible difference})$.

2.8 Cross-Region Analysis

To identify region-specific versus conserved expression patterns, we compared BLA and mPFC for shared interneuron and glial subclasses (8 in MERFISH, 10 in 10x). Excitatory neurons were excluded due to region-specific taxonomy (BLA glutamatergic types vs. cortical layer types). Mean expression and fraction expressing were computed per subclass in each region. Spearman correlations were calculated per gene (across cell types) and per cell type (across genes) to assess regional conservation. Log₂ fold-changes (BLA/mPFC) were computed for mean expression, with a pseudocount of 0.01 added to prevent division by zero. Differences in fraction expressing (BLA - mPFC) quantified region-specific prevalence. Cell-type rank order was compared between regions to identify receptors with conserved versus region-dependent cellular specificity.

2.9 Statistical Analysis and Software

All analyses were performed in Python 3.11. Key packages included: `abc_atlas_access` (0.1.0) for data retrieval, `anndata` (0.10.3) for expression matrix handling, `scanpy` (1.9.6) for dot plot generation, `pandas` (2.1.4) for data manipulation, `numpy` (1.26.2) for numerical operations, `scipy` (1.11.4) for correlation statistics, and `matplotlib` (3.8.2) for visualization. Spearman correlations were used as the primary association metric due to robustness against non-normal distributions and outliers.

3. Results

3.1 Cell type composition and data modalities

We analyzed neuromodulator receptor expression in the basolateral amygdala (BLA) and medial prefrontal cortex (mPFC) using two complementary data modalities from the Allen Brain Cell Atlas: 10x single-nucleus RNA sequencing (snRNA-seq) and MERFISH spatial transcriptomics. The 10x dataset provided whole-transcriptome coverage (28 receptor genes analyzed) across 4,042,976 cells, while the MERFISH dataset

offered spatially resolved expression with CCF-registered anatomical localization across 4,334,174 cells, albeit limited to 11 receptor genes present in the 550-gene MERFISH panel.

For the BLA, the 10x dataset yielded 28,809 neuronal cells comprising 18,938 excitatory neurons from two BLA-specific subclasses (LA-BLA-BMA-PA Glut with 16,778 cells and MEA-COA-BMA Ccdc42 Glut with 2,160 cells) and 9,871 GABAergic interneurons across 8 major subclasses (Sst Gaba 2,609 cells, Vip Gaba 2,081 cells, Pvalb Gaba 1,343 cells, Lamp5 Gaba 1,208 cells, Sncg Gaba 1,086 cells, Lamp5 Lhx6 Gaba 678 cells, Sst Chodl Gaba 448 cells, and Pvalb chandelier Gaba 418 cells). Including glia (19,140 astrocytes and 6,164 microglia from the CTXsp region), the total analyzed BLA dataset comprised 54,113 cells across 12 subclasses (**Figure 1**). A critical caveat is that GABAergic interneuron subclasses in the 10x data derive from the entire cortical subplate (CTXsp) dissection region and cannot be spatially localized to BLA versus neighboring structures (claustrum, endopiriform nucleus) based on transcriptomic identity alone. The MERFISH dataset addressed this limitation through CCF parcellation, yielding 8,238 cells with confirmed BLA localization (including 4,484 LA-BLA-BMA-PA Glut excitatory neurons, 1,676 interneurons across 6 subclasses, and 2,097 glia) distributed across three BLA substructures: anterior (BLAa, 5,933 cells), posterior (BLAp, 4,647 cells), and ventral (BLAv, 2,653 cells) (**Figure 5, Supplementary Figure S3**).

For the mPFC (prelimbic, infralimbic, and dorsal anterior cingulate areas), the 10x dataset provided 165,539 neuronal cells including 135,459 excitatory neurons across 10 layer-defined cortical subclasses (L6 CT CTX Glut 38,354 cells, L4/5 IT CTX Glut 23,357 cells, L6 IT CTX Glut 20,452 cells, L2/3 IT CTX Glut 18,401 cells, L5 IT CTX Glut 15,020 cells, L5 NP CTX Glut 7,529 cells, L5 ET CTX Glut 5,710 cells, L6b CTX Glut 3,295 cells, L2/3 IT RSP Glut 2,666 cells, and L4 RSP-ACA Glut 675 cells) and 30,080 GABAergic interneurons across 8 subclasses, resolving into 101 finer supertypes (**Figure 2, Supplementary Figure S2**). With glia (14,917 astrocytes and 6,823 microglia), the total mPFC 10x dataset comprised 187,279 cells across 20 subclasses. The MERFISH dataset provided 64,474 region-specific cells distributed across four cortical areas: anterior cingulate dorsal (ACAd, 25,482 cells), anterior cingulate ventral (ACAv, 27,707 cells), prelimbic (PL, 18,243 cells), and infralimbic (ILA, 7,084 cells) (**Figure 6, Supplementary Figure S4**).

The MERFISH gene panel captured 5 of 14 serotonin receptors (Htr1b, Htr1d, Htr2a, Htr3a, Htr7; missing Htr1a, Htr1f, Htr2b, Htr2c, Htr3b, Htr4, Htr5a, Htr5b, Htr6), 2 of 9 noradrenergic receptors (Adra1a, Adra1b; missing Adra1d, Adra2a/b/c, Adrb1/2/3), and 4 of 5 dopamine receptors (Drd1, Drd2, Drd3, Drd5; missing Drd4), limiting cross-modality comparisons to these 11 genes but enabling spatially resolved validation of the most critical targets identified in the 10x data.

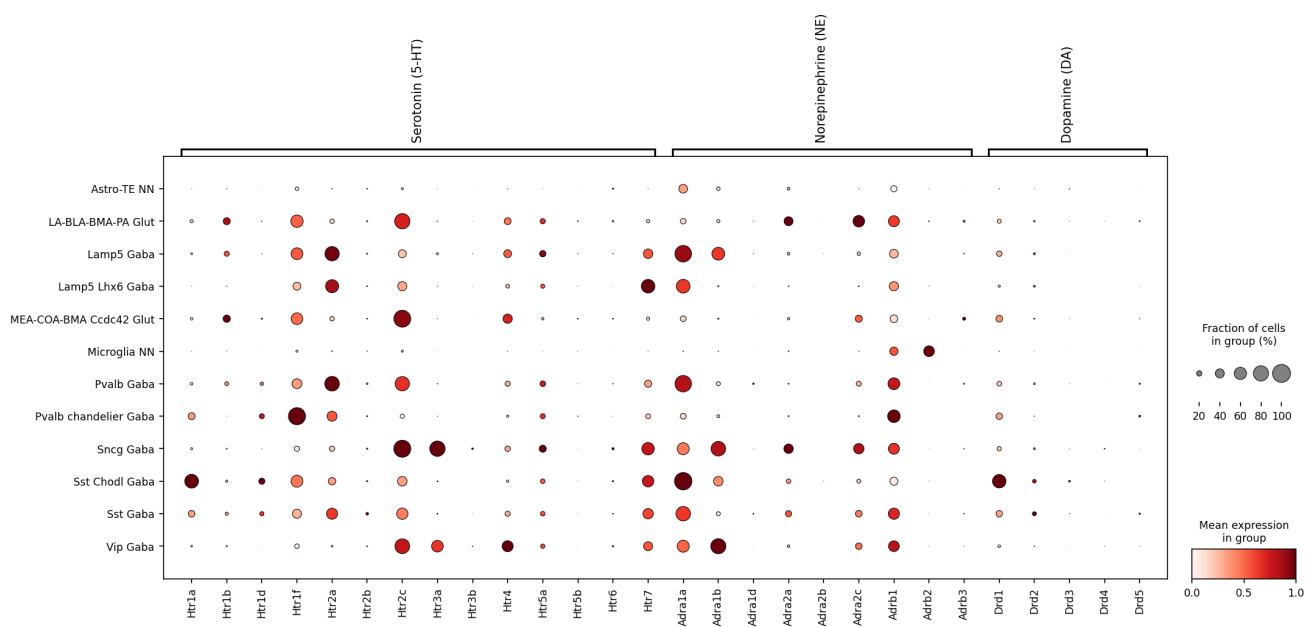


Figure 1. Neuromodulator receptor expression in BLA cell types (10x scRNA-seq). Dot plot showing expression of 28 neuromodulator receptor genes across 12 cell types in the basolateral amygdala, including 2 excitatory neuron subclasses, 8 GABAergic interneuron subclasses, and 2 glial types. Data represent 54,113 cells from the CTXsp dissection region. Dot color indicates mean log₂-normalized expression (variance-scaled per gene); dot size indicates fraction of cells with detectable expression.

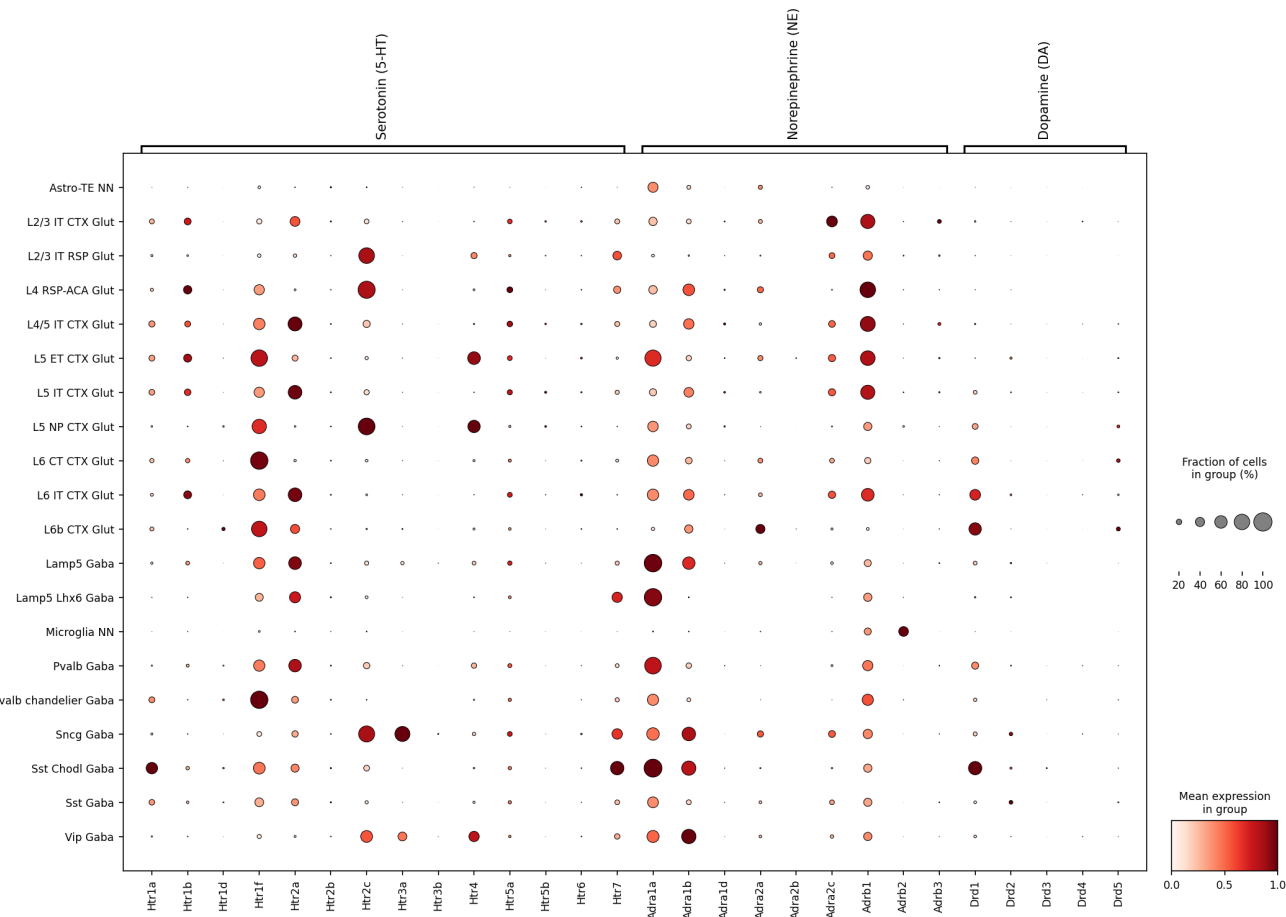


Figure 2. Neuromodulator receptor expression in mPFC cell types (10x scRNA-seq). Dot plot showing expression of 28 receptor genes across 20 cell types in the medial prefrontal cortex, including 10 excitatory layer types and 10 GABAergic/glial types. Data represent 187,279 cells from PL-ILA-ORB and ACA dissection regions.

3.2 Serotonin receptor expression patterns

Htr2a, the primary target of classic psychedelics including psilocybin and LSD, exhibited robust and highly cell-type-specific expression patterns that were remarkably consistent across brain regions and data modalities. In the BLA, 10x data revealed highest Htr2a expression in parvalbumin-positive interneurons (Pvalb Gaba: mean log₂ expression 5.17, fraction expressing 75.9%) and Lamp5 interneurons (5.07, 74.0%), with moderate expression in excitatory neurons (LA-BLA-BMA-PA Glut: 0.91, 15.8%) (**Figure 1**). MERFISH spatial data confirmed this pattern with strong Htr2a signal in Pvalb (2.33, 94.4%) and Lamp5 (2.13, 92.0%) interneurons spatially localized within BLA substructures (**Supplementary Figure S3**). In the mPFC, Htr2a expression was prominent across multiple cortical layers, particularly in deep-layer intratelencephalic neurons (L4/5 IT CTX Glut: 4.68, 69.8%; L5 IT CTX Glut: 4.61, 67.6%; L6 IT CTX Glut: 4.55, 67.6%) and parvalbumin interneurons (4.00, 60.5%) (**Figure 2**). Notably, the superficial layer neurons that send cortico-amygda projections

showed moderate expression (L2/3 IT CTX Glut: 2.68, 43.6%). Cross-modality validation demonstrated strong agreement between 10x and MERFISH platforms, with Spearman correlation coefficients of rho=0.964 for BLA and rho=0.953 for mPFC when comparing cell-type-specific expression profiles (**Figure 3**, **Supplementary Figure S5**). Cross-region comparison revealed largely conserved Htr2a expression patterns across shared interneuron types (MERFISH cross-region rho=0.929), with modest enrichment in BLA Pvalb interneurons relative to mPFC (**Figure 4**).

Htr1a, the high-affinity 5-HT1A autoreceptor and heteroreceptor implicated in modulating psychedelic responses and anxiolytic drug action, was absent from the MERFISH panel but showed distinctive expression patterns in the 10x data. The highest Htr1a expression was observed in somatostatin-positive interneurons, particularly the Sst Chodl subclass (BLA: 4.50, 70.3%; mPFC: 3.46, 53.6%) and parvalbumin chandelier cells (BLA: 1.59, 28.7%; mPFC: 1.34, 22.3%), with broader moderate expression across cortical Sst interneurons (BLA: 1.54, 26.6%; mPFC: 1.24, 20.8%) (**Figures 1-2**). In mPFC, Htr1a also showed notable expression in superficial and middle-layer excitatory neurons (L4/5 IT: 1.28, 23.7%; L5 IT: 1.17, 21.5%). This distribution positions Htr1a-expressing interneurons to modulate circuit gain and potentially shape psychedelic-induced cortical dynamics through GABAergic inhibition.

Htr2c, which opposes Htr2a signaling in anxiety circuits and is targeted by the FDA-approved anti-obesity drug lorcaserin, exhibited strikingly high and cell-type-selective expression that was also absent from the MERFISH panel. The most dramatic Htr2c enrichment occurred in Sncg interneurons (BLA: 8.74, 93.2%; mPFC: 7.04, 84.1%), a neurogliaform-like population of CGE-derived interneurons known for dense local inhibition (**Figures 1-2**). L5 near-projecting neurons (L5 NP CTX Glut) in mPFC showed exceptionally high expression (8.15, 88.9%), as did retrosplenial-projecting L2/3 and L4 neurons in anterior cingulate regions (L2/3 IT RSP Glut: 7.05, 81.4%; L4 RSP-ACA Glut: 6.95, 91.7%). BLA excitatory neurons displayed strong expression (LA-BLA-BMA-PA Glut: 6.45, 80.8%; MEA-COA-BMA Ccdc42 Glut: 8.20, 92.3%), with substantial expression also in Vip (BLA: 6.87, 76.9%; mPFC: 4.59, 56.2%) and Pvalb interneurons (BLA: 5.95, 74.1%). Cross-region analysis revealed significant BLA enrichment for Htr2c (mean log₂ fold-change +1.604), making it the most region-differentiated serotonin receptor (**Figure 4, Supplementary Figure S7**).

Htr7, a Gs-coupled receptor implicated in fear extinction and circadian regulation, showed highest expression in deep-layer corticothalamic and cortico-tectal projection neurons (mPFC: L6 CT CTX Glut 7.60, 93.5%; L6b CTX Glut 6.24, 80.2%; L5 ET CTX Glut 6.35, 87.1%) and parvalbumin chandelier cells (BLA: 7.66, 93.8%; mPFC: 7.80, 93.3%) in the 10x data (**Figures 1-2**). Moderate expression was also observed in Sst Chodl interneurons and L5 NP neurons (5.46, 72.5%). MERFISH data confirmed Htr7 expression in Sst interneurons and projection neuron populations, with Spearman correlations of rho=0.745 (BLA) and rho=0.816 (mPFC) between modalities (**Figure 3**). Notably, Htr7 showed significant BLA enrichment across shared cell types (10x cross-region log₂ FC +0.681, MERFISH +0.693), suggesting potential region-specific contributions to amygdala-dependent fear extinction (**Figure 4**).

Htr3a, a marker of CGE-derived interneurons and the only ionotropic serotonin receptor, showed highly selective expression in Sncg (BLA 10x: 6.44, 81.0%; mPFC 10x: 6.14, 76.8%; BLA MERFISH: 2.87, 76.4%; mPFC MERFISH: 3.71, 86.9%) and Vip interneurons (BLA 10x: 4.17, 56.5%; mPFC 10x: 2.84, 37.7%; BLA MERFISH: 2.47, 86.4%; mPFC MERFISH: 2.36, 82.2%) across all datasets (**Figures 1-2, Supplementary Figures S3-S4**). This pattern was among the most reproducible across modalities (BLA rho=0.685, mPFC rho=0.890) and regions (MERFISH rho=0.714), consistent with Htr3a's established role as a canonical CGE interneuron marker.

Additional serotonin receptors showed more restricted or lower expression. Htr1b was moderately expressed in excitatory neurons (BLA: LA-BLA-BMA-PA Glut 1.61, 28.6%; mPFC: L2/3 IT 1.56, 27.1%) with excellent cross-modality agreement (BLA rho=0.879, mPFC rho=0.914). Htr1d showed sparse expression overall but displayed the most variable cross-modality concordance (BLA rho=0.285, mPFC rho=0.571), likely reflecting its generally low transcript levels approaching technical detection limits. Htr1f, Htr2b, Htr3b, Htr4, Htr5a/b, and Htr6 (all 10x-only) showed minimal expression across most cell types, with Htr1f notable as a moderate marker of projection neurons and Htr4 enriched in L5 ET and L5 NP neurons.

3.3 Noradrenergic receptor expression patterns

The beta-1-adrenergic receptor (Adrb1), the primary target of the beta-blocker propranolol used to treat anxiety and prevent fear memory reconsolidation, exhibited dominant expression in excitatory neurons with a strong mPFC bias. In mPFC, Adrb1 showed high expression across all cortical layers (L4/5 IT: 4.96, 76.7%; L2/3 IT: 4.64, 71.4%; L5 IT: 4.55, 70.9%; L5 ET: 4.60, 74.2%; L6 IT: 3.85, 61.6%), with lower but detectable expression in interneurons (**Figure 2**). BLA excitatory neurons showed more moderate Adrb1 expression (LA-BLA-BMA-PA Glut: 2.95, 52.1%), with interneurons expressing at similar or higher levels (Pvalb chandelier: 3.71, 62.2%; Vip: 3.33, 50.4%; Sst: 3.11, 53.3%) (**Figure 1**). Cross-region analysis confirmed significant mPFC enrichment for Adrb1 ($\log_2 FC -0.354$), potentially underlying region-specific noradrenergic modulation of prefrontal executive function versus amygdala threat processing.

Alpha-1 adrenergic receptors Adra1a and Adra1b, Gq-coupled receptors mediating noradrenergic excitation, displayed complementary expression patterns favoring GABAergic interneurons. Adra1a showed highest expression in Lamp5 interneurons across both regions (BLA 10x: 4.37, 57.2%; BLA MERFISH: 0.99, 70.8%; mPFC MERFISH: 1.58, 82.5%) and Pvalb interneurons (BLA MERFISH: 0.81, 58.4%; mPFC MERFISH: 1.42, 81.0%), with notable enrichment in mPFC Sst Chodl (10x: 1.73, 88.2%) and Lamp5 Lhx6 populations (MERFISH: 2.14, 93.6%). Adra1b was most prominently expressed in Vip interneurons (BLA 10x: 2.18, 88.9%; mPFC 10x: 2.88, 95.8%), Lamp5 interneurons (BLA 10x: 1.41, 88.3%), and Sncg interneurons (BLA 10x: 1.51, 80.6%), with strong enrichment in mPFC relative to BLA (MERFISH $\log_2 FC -1.215$, the largest regional difference observed for any receptor). These patterns suggest that noradrenergic modulation via alpha-1 receptors preferentially targets inhibitory microcircuits, with Adra1a favoring neurogliaform-like Lamp5 populations and Adra1b favoring disinhibitory Vip and Sncg interneurons.

Alpha-2 adrenergic receptors, which are Gi-coupled inhibitory receptors absent from the MERFISH panel, showed more restricted expression in the 10x data. Adra2c was moderately expressed in BLA excitatory neurons (LA-BLA-BMA-PA Glut: 3.21, 55.6%) and Sncg interneurons (2.71, 48.3%), with lower mPFC expression (L2/3 IT: 2.87, 49.8%; L5 IT: 1.59, 28.8%), resulting in significant BLA enrichment (\log_2 FC +0.925). Adra2a showed even stronger BLA bias (\log_2 FC +1.118), with preferential expression in BLA excitatory and interneuron populations. These Gi-coupled alpha-2 receptors may mediate presynaptic autoinhibition of norepinephrine release and postsynaptic inhibition, with their BLA enrichment potentially contributing to region-specific noradrenergic modulation of threat processing. The beta-2 and beta-3 adrenergic receptors (Adrb2, Adrb3) showed minimal expression across cell types, and Adra1d expression was sparse.

3.4 Dopamine receptor expression patterns

D1-like dopamine receptors (Drd1, Drd5) showed prominent expression in deep cortical layers and select interneuron populations. Drd1 was most highly expressed in Sst Chodl interneurons (BLA 10x: 4.25, 68.1%; mPFC 10x: 4.12, 65.6%; mPFC MERFISH: 2.37, 86.8%), deep-layer projection neurons (mPFC 10x: L6b 3.86, 59.3%; L6 IT 2.95, 49.1%; L6 CT 1.75, 29.7%; MERFISH: L6b 2.50, 89.3%; L6 IT 1.90, 87.9%; L6 CT 1.46, 76.6%), and BLA excitatory neurons (MEA-COA-BMA Ccdc42 Glut 10x: 1.64, 27.2%; MERFISH: 1.16, 70.1%). Cross-modality agreement for Drd1 was excellent (BLA rho=0.794, mPFC rho=0.927), supporting high confidence in this expression pattern (**Figure 3**). Drd5 showed a similar but more restricted pattern, with highest expression in deep-layer neurons. The enrichment of D1-like receptors in deep layers suggests preferential dopaminergic modulation of cortico-subcortical projection pathways originating from L5 ET, L6 CT, and L6b neurons.

D2-like receptors showed more selective expression favoring specific GABAergic populations. Drd2 was most prominently expressed in Sst interneurons (BLA 10x: 0.75, 13.5%; mPFC 10x: 0.72, 12.1%; BLA MERFISH: 0.44, 32.2%; mPFC MERFISH: 0.56, 37.6%), Sst Chodl (mPFC 10x: 0.36, 5.7%; MERFISH: 0.49, 36.8%), and Sncg interneurons (BLA 10x: 0.30, 5.4%; mPFC 10x: 0.65, 11.2%; mPFC MERFISH: 0.44, 28.9%). Cross-region comparison revealed significant BLA enrichment for Drd2 (10x \log_2 FC +0.630), suggesting enhanced dopaminergic inhibition of GABAergic microcircuits in the amygdala relative to prefrontal cortex. Drd3 showed minimal expression overall, with highest levels in Sst Chodl interneurons. Drd4, absent from the MERFISH panel, showed sparse expression in the 10x data across all cell types.

3.5 Cross-modality validation of receptor expression patterns

To assess the robustness of cell-type-specific receptor expression patterns across measurement platforms, we systematically compared 10x snRNA-seq and MERFISH spatial transcriptomics data for the 11 shared receptor genes across matched cell types. Overall correlation between modalities was strong, with Spearman correlation coefficients for fraction of cells expressing each receptor of rho=0.788 for BLA and rho=0.884 for mPFC across all gene x cell type combinations (**Figure 3A-B**). Mean expression levels showed similar concordance (BLA rho=0.758, mPFC rho=0.859), though with greater variance attributable to the technical differences

between nuclear (10x) versus whole-cell (MERFISH) RNA capture and the more limited dynamic range of the targeted MERFISH panel.

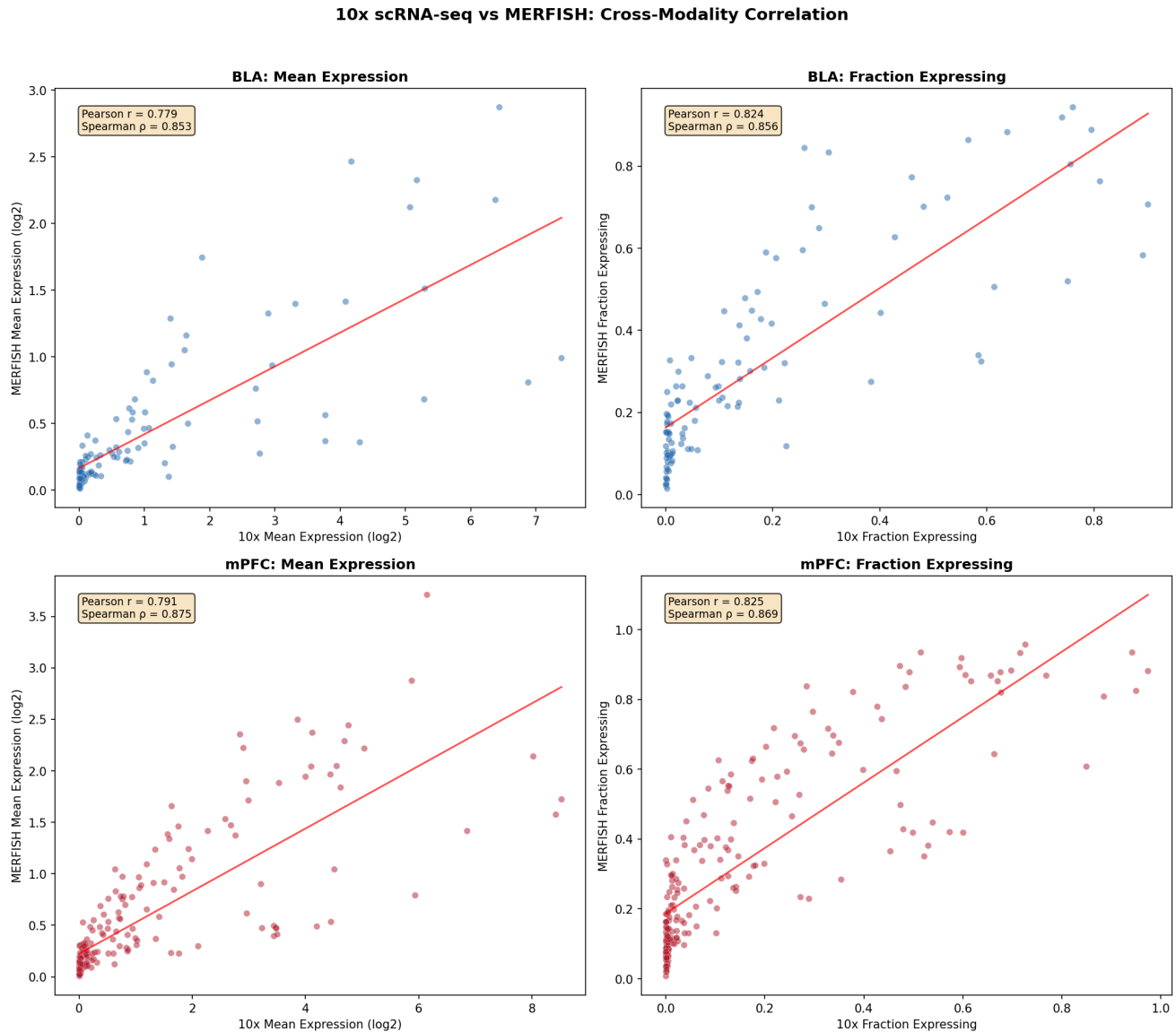


Figure 3. Cross-modality validation of receptor expression (10x vs. MERFISH). Scatter plots comparing mean expression and fraction expressing for 11 shared receptor genes across matched cell types, separately for BLA and mPFC. Each point represents one gene x cell type combination. Pearson and Spearman correlation coefficients are displayed.

Per-gene analysis revealed highly consistent cross-platform agreement for most receptors, with per-cell-type expression patterns correlating at $\rho \geq 0.8$ for the majority of genes (**Supplementary Figure S5**). Htr2a showed the strongest cross-modality concordance (BLA $\rho=0.964$, mPFC $\rho=0.953$), followed by Adra1b (BLA $\rho=0.685$, mPFC $\rho=0.926$), Drd1 (BLA $\rho=0.794$, mPFC $\rho=0.927$), Htr1b (BLA $\rho=0.879$, mPFC

$\rho=0.914$), and Htr3a (BLA $\rho=0.685$, mPFC $\rho=0.890$). The weakest cross-platform agreement was observed for Htr1d (BLA $\rho=0.285$, mPFC $\rho=0.571$) and Drd3 (BLA $\rho=0.467$, mPFC $\rho=0.600$), likely reflecting sparse expression approaching technical noise floors in both platforms.

Per-cell-type analysis demonstrated that glial populations showed the strongest cross-platform concordance (astrocytes: BLA $\rho=0.982$, mPFC $\rho=0.991$; microglia: BLA $\rho=0.927$, mPFC $\rho=0.945$), likely due to their highly distinctive expression signatures and larger cell sizes favoring MERFISH detection. Among neuronal populations, mPFC excitatory neurons showed excellent agreement (L6 IT $\rho=0.924$, L4/5 IT $\rho=0.909$, L2/3 IT $\rho=0.897$), as did most mPFC interneurons (Vip $\rho=0.964$, Sncg $\rho=0.903$, Lamp5 $\rho=0.873$). BLA cell types showed somewhat lower but still substantial concordance, with the somewhat weaker BLA correlations likely reflecting the confounding effect that BLA interneurons in the 10x dataset derive from the entire CTXsp dissection region rather than being spatially restricted to BLA as in the MERFISH data.

Consensus receptor rankings, computed by averaging cell-type ranks across both modalities and weighting by cross-platform agreement, identified 55 high-confidence gene x cell type combinations (consensus rank ≤ 3 , confidence ≥ 0.7) that showed minimal rank discordance between platforms (**Supplementary Figure S6**). For Htr2a, high-confidence top-ranked cell types included BLA Pvalb and Lamp5 interneurons and mPFC L4/5 IT and L6 IT excitatory neurons. For Htr3a, Sncg and Vip interneurons ranked first in both regions with perfect cross-platform agreement. Drd1 showed consistent top rankings in deep-layer neurons (L6b, L6 IT, L6 CT) and Sst Chodl interneurons. These consensus rankings provide experimentally validated targets for pharmacological and genetic manipulation studies.

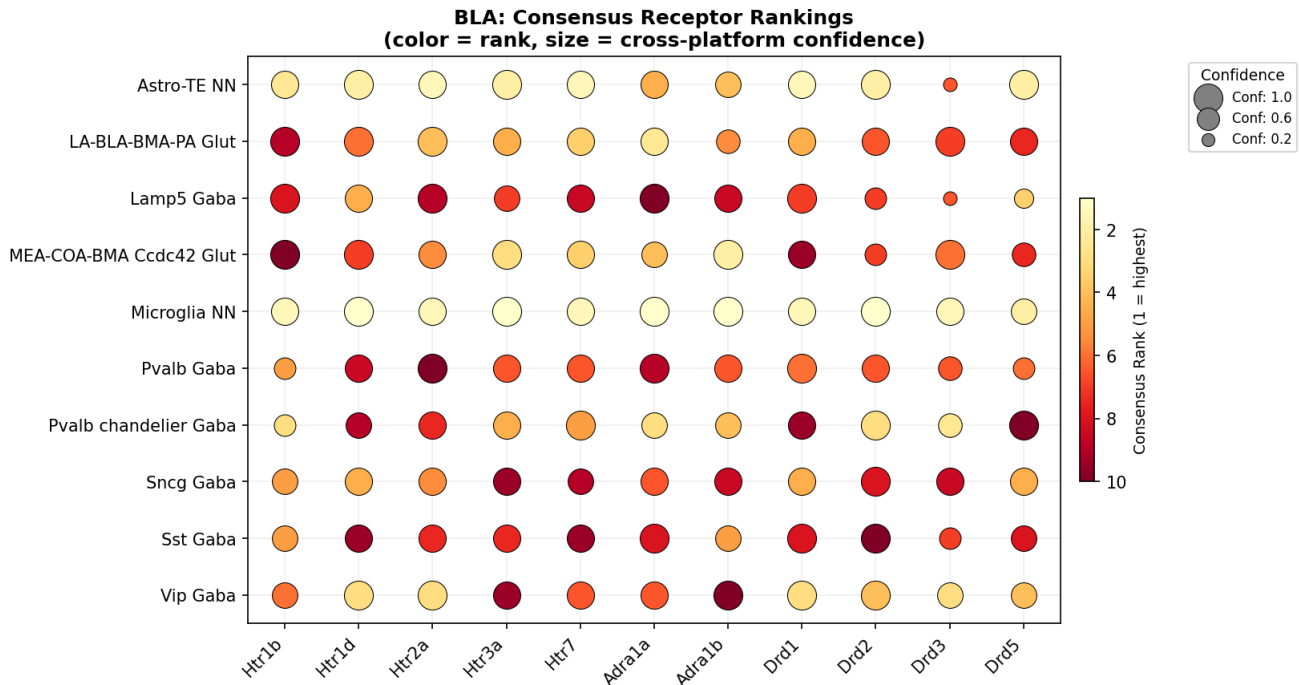


Figure 3C. Consensus receptor rankings for BLA. Dot color indicates consensus rank (1 = highest expression, darker = higher rank); dot size indicates cross-platform confidence.

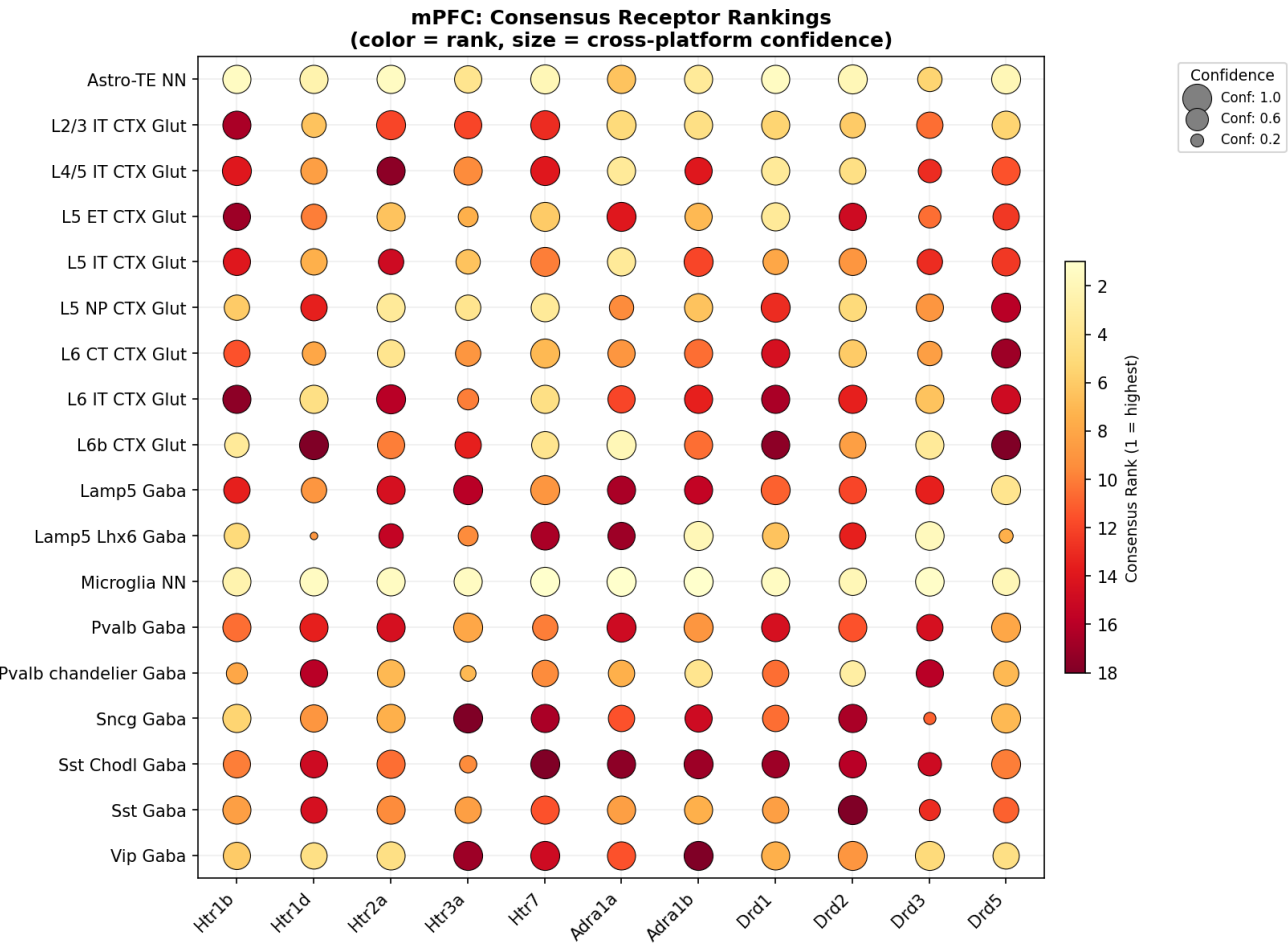


Figure 3D. Consensus receptor rankings for mPFC. High-confidence top rankings (large, dark dots) represent the most reproducible expression patterns suitable for experimental validation.

3.6 Cross-region comparison of receptor expression in shared cell types

To identify conserved versus region-specific receptor expression patterns, we compared BLA and mPFC expression profiles for the 8 interneuron and glial subclasses shared between regions in the MERFISH dataset and the 10 shared subclasses in the 10x dataset. Overall cross-region correlation for shared cell types was moderate (MERFISH: fraction expressing rho=0.587, mean expression rho=0.570; 10x: rho=0.728, rho=0.714), substantially lower than cross-modality correlations within regions, indicating significant region-specific tuning of receptor expression despite shared cell-type identities (**Figure 4A-B**).

Cross-Region: BLA vs mPFC (MERFISH, shared interneurons + glia)

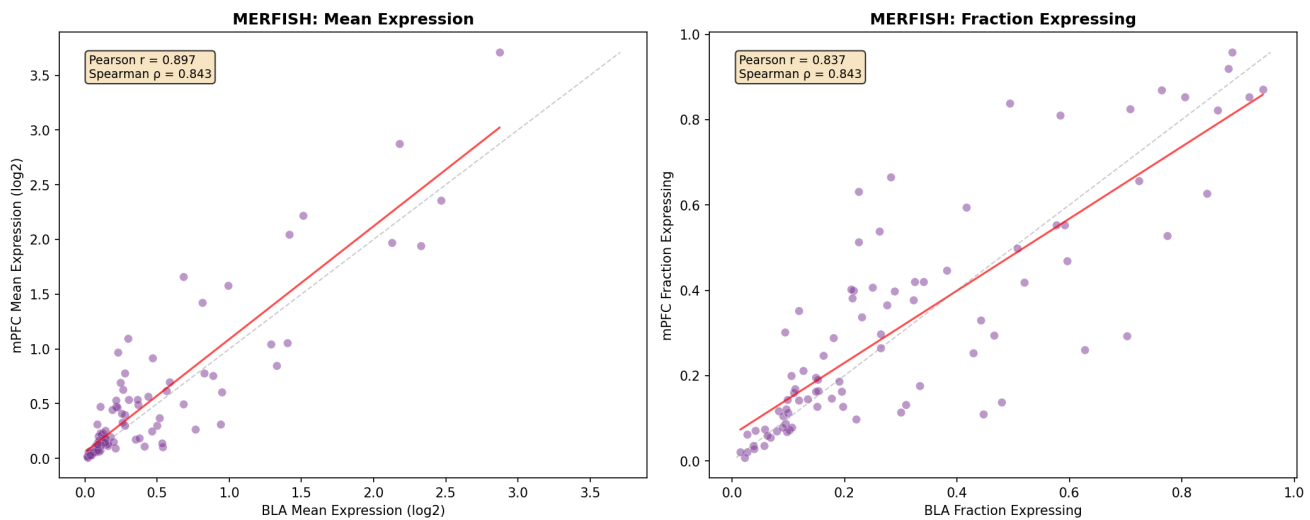


Figure 4A. Cross-region comparison (MERFISH). Scatter plot comparing fraction expressing in BLA versus mPFC for shared interneuron and glial types (8 shared types, 11 genes).

Cross-Region: BLA vs mPFC (10x scRNA-seq, shared interneurons + glia)

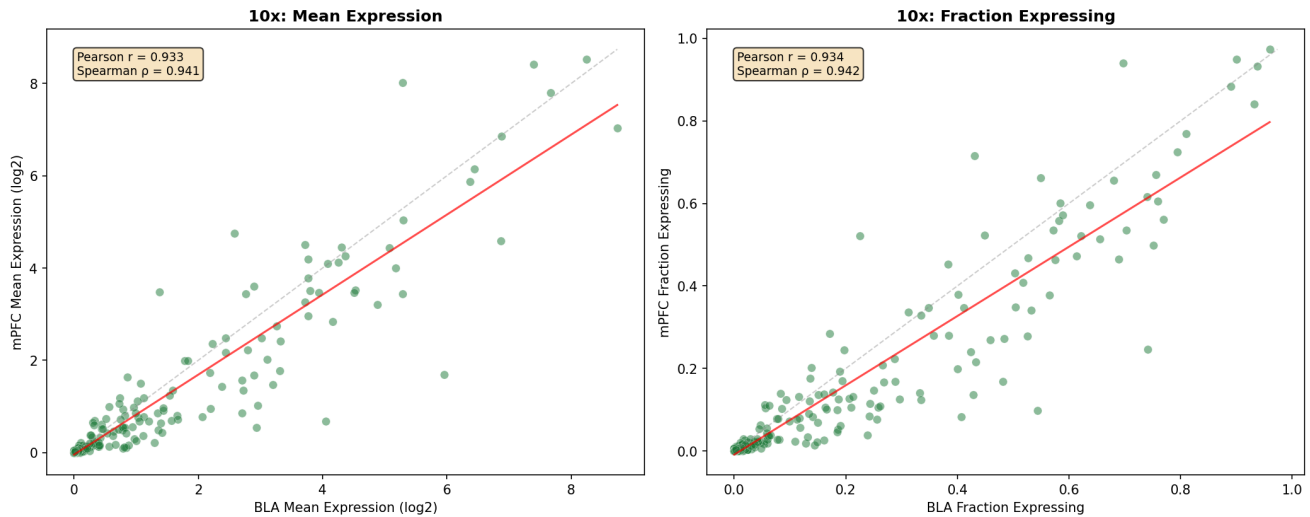


Figure 4B. Cross-region comparison (10x). Scatter plot comparing fraction expressing in BLA versus mPFC for shared types (10 shared types, 28 genes).

Several receptors showed highly conserved expression patterns across regions, particularly Htr2a (MERFISH cross-region rho=0.929), Htr3a (rho=0.714), and Drd1 (rho=0.762), reflecting cell-type-intrinsic expression programs maintained across brain areas. These conserved patterns suggest that psychedelic drug effects mediated by Htr2a and neuromodulation via Htr3a likely engage similar interneuron microcircuits across limbic and prefrontal regions.

In contrast, multiple receptors exhibited significant region-specific enrichment. In the 10x dataset, Htr2c showed the strongest BLA enrichment (mean log2 fold-change across shared cell types: +1.604, with 9 of 10 cell types higher in BLA), particularly in excitatory neurons and Sncg interneurons. Other BLA-enriched receptors included Htr1d (+1.086), Adra2a (+1.118), Adra2c (+0.925), Htr4 (+0.874), Htr7 (+0.681), and Drd2 (+0.630), with MERFISH data independently confirming Htr7 enrichment (+0.693) and Htr1d enrichment (+0.722). The consistent BLA bias for Htr2c and Adra2a/c across interneuron populations suggests enhanced serotonergic and noradrenergic inhibitory modulation in amygdala circuits, potentially contributing to the amygdala's role in threat detection and anxiety.

Conversely, several receptors showed mPFC enrichment. Adra1b displayed strong mPFC bias in the MERFISH data (log2 FC -1.215, the largest regional difference for any receptor), particularly in Vip interneurons, Sst Chodl, and excitatory neurons. The 10x data similarly showed mPFC enrichment for Adra1a (-0.292) and Adra1b (-0.306). Adrb1 was also mPFC-enriched (+0.354), consistent with the preferential expression in mPFC excitatory neurons noted above.

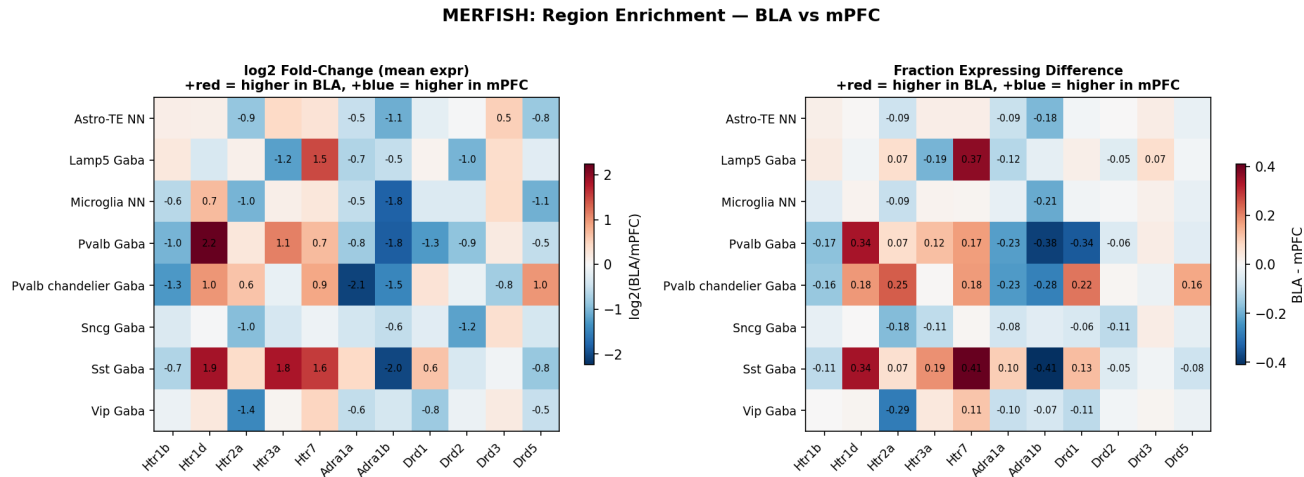


Figure 4C. Regional enrichment heatmap (MERFISH). Log2 fold-change of BLA/mPFC expression. Red indicates BLA-enriched; blue indicates mPFC-enriched.

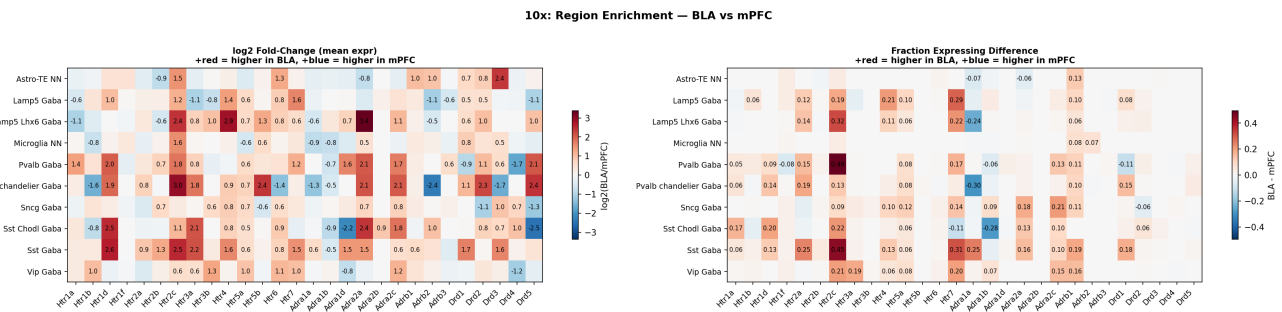


Figure 4D. Regional enrichment heatmap (10x). Htr2c, Adra2a, and Htr4 are robustly BLA-enriched across multiple cell types.

Glia showed generally conserved receptor profiles across regions, with astrocytes displaying minimal regional differences for most receptors and microglia showing low expression overall. This regional invariance in glial receptor expression contrasts with the substantial neuronal heterogeneity.

3.7 Spatially resolved receptor expression within BLA and mPFC substructures

The MERFISH dataset enabled analysis of receptor expression gradients across anatomically defined substructures within each region. In the BLA, we examined expression across anterior (BLAa), posterior (BLAp), and ventral (BLAv) subdivisions. While most receptors showed relatively uniform expression across BLA subdivisions within each cell type, several patterns emerged (**Figure 5**). Excitatory LA-BLA-BMA-PA Glut neurons showed modest anterior-posterior gradients for select receptors: Htr2a expression was highest in BLAa (mean 0.35, fraction 0.32) with progressive decreases toward BLAp (0.33, 0.30) and BLAv (0.24, 0.25). Drd1 showed a complementary pattern with highest expression in BLAp and BLAv.

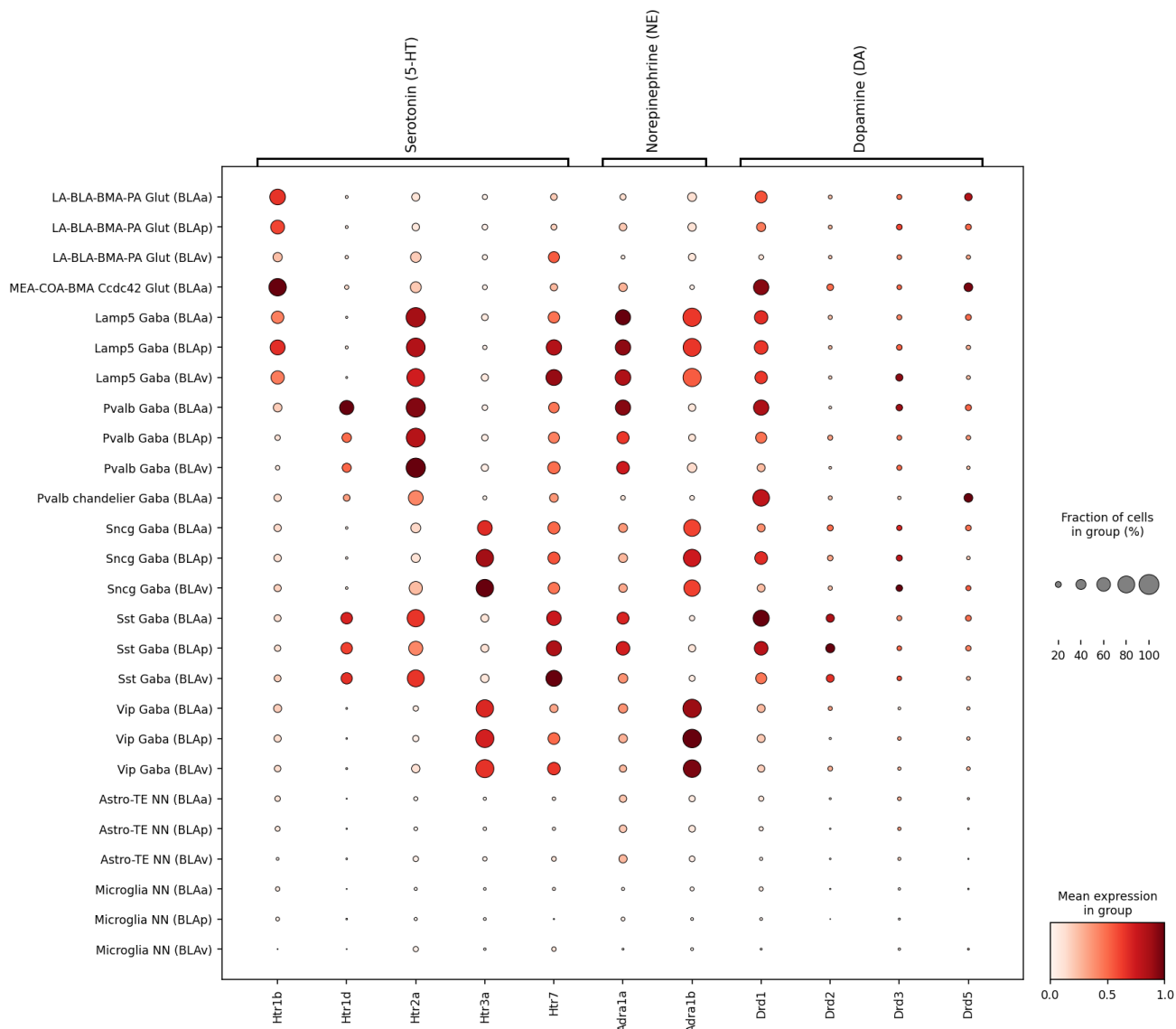


Figure 5. Spatial heterogeneity of BLA receptor expression (MERFISH). Dot plot showing expression of 11 MERFISH receptor genes across BLA cell types subdivided by anatomical substructure (BLAa, BLAp, BLAv). Data represent 8,238 spatially resolved cells.

Within the mPFC, we analyzed expression across prelimbic (PL), infralimbic (ILA), dorsal anterior cingulate (ACAd), and ventral anterior cingulate (ACAv) areas (**Figure 6**). L2/3 IT neurons showed relatively uniform Htr2a expression across all four areas (PL: 1.47, 0.74; ILA: 1.52, 0.77; ACAd: 1.43, 0.73; ACAv: 1.49, 0.75). Deep-layer neurons (L6 CT, L6 IT, L6b) displayed more pronounced area differences for Drd1, with enhanced expression in PL and ACA regions relative to ILA, potentially reflecting area-specific dopaminergic modulation of cortico-thalamic feedback. The preservation of cell-type-specific receptor signatures across mPFC subdivisions suggests that the molecular identity of neuronal subtypes is largely conserved, while

quantitative expression differences may contribute to functional specialization of prelimbic, infralimbic, and cingulate circuits in fear expression, extinction, and conflict monitoring, respectively.

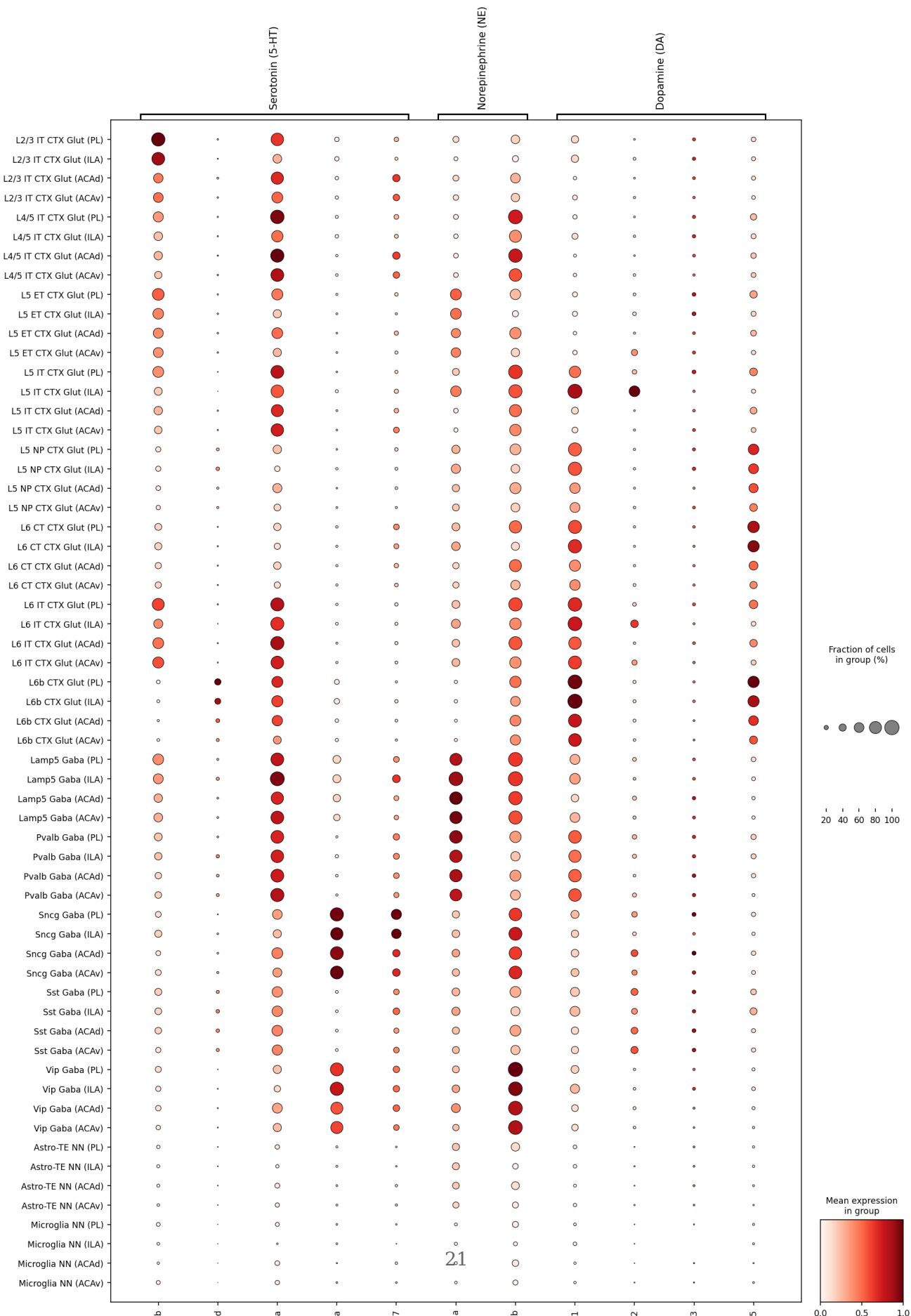


Figure 6. Spatial heterogeneity of mPFC receptor expression (MERFISH). Dot plot showing expression of 11 receptor genes across mPFC cell types subdivided by prefrontal area (PL, ILA, ACAd, ACAv). Data represent 64,474 spatially resolved cells.

4. Discussion

Our systematic characterization of neuromodulator receptor expression across BLA and mPFC cell types reveals several findings with direct implications for understanding psychedelic mechanisms, anxiolytic drug action, and the cellular substrates of monoaminergic circuit modulation.

The psychedelic-relevant serotonin receptors show striking cell-type specificity that helps explain the complex phenomenology and therapeutic mechanisms of 5-HT2A agonists. Htr2a expression is highest in cortical excitatory neurons, particularly the superficial layer 2/3 intratelencephalic (IT) and layer 4/5 IT populations in the mPFC. This aligns with extensive prior evidence that psychedelics primarily activate cortical pyramidal neurons and that cortical 5-HT2A receptor density predicts psychedelic potency. Notably, Htr2a is also robustly expressed in specific interneuron subtypes, particularly Lamp5 and Pvalb populations in both regions, suggesting that psychedelics can directly modulate inhibitory as well as excitatory transmission. In the BLA, the pattern shifts: while excitatory neurons show moderate Htr2a expression, Pvalb and Lamp5 interneurons express particularly high levels, suggesting that psychedelic modulation of the BLA may operate more through disinhibitory mechanisms than through direct excitation of principal neurons. This could contribute to the emotional intensification and fear memory reactivation that can occur during psychedelic-assisted therapy.

The Htr1a receptor, captured in the 10x data but not in MERFISH, shows highest expression in specialized interneuron subtypes including Sst Chodl and Pvalb chandelier cells. The 5-HT1A receptor is Gi-coupled and generally inhibitory, and it has long been recognized as an anxiolytic target and a modulator of psychedelic effects. The high expression in cholecystokinin-expressing somatostatin interneurons and chandelier cells—both of which target specific subcellular domains of pyramidal neurons—suggests that 5-HT1A activation may fine-tune the temporal dynamics of excitation in ways that buffer against excessive 5-HT2A-mediated depolarization. This could explain why 5-HT1A partial agonists like buspirone produce anxiolytic effects without psychedelic phenomenology, and why polymorphisms in HTR1A influence individual responses to psychedelics in humans.

Perhaps the most striking finding is the extremely high expression of Htr2c in specific subclasses. In the mPFC, layer 5 near-projecting (L5 NP) neurons, Sncg-expressing interneurons, and Vip populations show the highest Htr2c levels. In the BLA, Htr2c expression is even more pronounced, with Sncg, Vip, and LA-BLA-BMA-PA excitatory populations showing the highest expression in our dataset. The 5-HT2C receptor is Gq-coupled like 5-HT2A, but the two receptors often have opposing functional effects, and 5-HT2C activation is associated with increased anxiety, reduced impulsivity, and modulation of appetite. Many atypical antipsychotics and some antidepressants show inverse agonism at 5-HT2C receptors, and this property may

contribute to their therapeutic effects. The intense Htr2c expression in BLA excitatory neurons suggests that this receptor may be particularly important for amygdala-dependent anxiety, and that drugs with different 5-HT2A/5-HT2C selectivity ratios may produce very different anxiolytic versus psychedelic effects. The concentration of Htr2c in Sncg and Vip interneurons, which are involved in disinhibitory circuits, further suggests complex interactions between 5-HT2A and 5-HT2C signaling in circuit state regulation.

Htr7 expression shows a more distributed pattern, with moderate levels across many cell types but highest expression in Sst Chodl and Lamp5 Lhx6 interneurons. While less studied than other serotonin receptors, 5-HT7 has emerged as a novel target for fear extinction facilitation and rapid antidepressant effects. The enrichment in specific interneuron subtypes that regulate rhythmic activity and temporal coordination suggests that 5-HT7 may modulate circuit oscillations and spike timing in ways that promote synaptic plasticity during extinction learning.

The noradrenergic receptor findings similarly reveal cell-type specificity relevant to clinical interventions. Adrb1 is the dominant adrenergic receptor in excitatory neurons across both regions, consistent with the effects of propranolol on fear memory consolidation and reconsolidation, which depend on plasticity in excitatory synapses. In contrast, Adra1a and Adra1b show preferential expression in interneuron subtypes, particularly Lamp5 and Pvalb populations, and this pattern is especially clear in the MERFISH spatial data. This suggests that alpha-1 receptor blockade with prazosin may exert its effects primarily through modulation of inhibitory tone rather than direct suppression of principal neuron activity. Adra2c shows interesting region- and layer-specific patterns, with higher expression in mPFC layer 2/3 neurons than in BLA, potentially explaining regional differences in sensitivity to alpha-2 agonists. The generally low expression of Adra2a in our dataset may reflect its predominant role as an autoreceptor on noradrenergic terminals rather than as a postsynaptic receptor in BLA and mPFC neurons.

The strong correlations between 10x snRNA-seq and MERFISH expression profiles (Spearman rho approximately 0.85-0.87) provide important validation that cell-type-specific receptor rankings are robust across platforms. The two technologies have different strengths and limitations—10x provides deeper transcript coverage and can detect lower-abundance mRNAs like Htr1a, while MERFISH provides spatial context and precisely localized cell type assignments—but they converge on similar rank orderings of which cell types express which receptors most highly. This cross-platform agreement increases confidence that the patterns we observe reflect genuine biological cell-type specificity rather than technical artifacts.

Cross-region comparisons reveal that interneuron receptor profiles are remarkably conserved between BLA and mPFC, with correlation coefficients around 0.94 in the 10x data. This suggests that the molecular logic of monoaminergic modulation of inhibitory circuits is similar across these structures, despite their different anatomical origins and circuit roles. Notable exceptions include Htr2c, which is higher in BLA interneurons, and Drd1, which shows higher expression in mPFC deep layer neurons. These regional differences may contribute to the distinct computational functions of these structures—the BLA's role in rapid threat detection versus the mPFC's role in sustained cognitive control.

The MERFISH spatial data allowed us to examine whether receptor expression varies systematically across anatomical subdivisions. For most receptors, expression is remarkably uniform across these subdivisions within each major region, suggesting that receptor density is more a function of cell type than of precise anatomical location. This spatial homogeneity simplifies interpretation: knowing the cell-type composition of a region is sufficient to predict its receptor profile without requiring detailed sub-regional parcellation.

Several limitations must be acknowledged. The MERFISH data do not include Htr1a or Htr2c in the measured gene panel, limiting our ability to spatially validate these important psychedelic-relevant receptors. The 10x BLA interneuron populations are derived from the broader CTXsp (cortical subplate) dissection, which includes cortical structures adjacent to the amygdala, and may not fully capture BLA-specific interneuron subtypes if they exist. Transcript expression does not equal protein expression or functional receptor density, and post-transcriptional regulation, trafficking, and desensitization can all modulate receptor availability. These are mouse data, and while receptor expression patterns are generally conserved across mammals, human-mouse differences in receptor pharmacology and expression are known for several genes. Finally, our analysis does not incorporate information about circuit connectivity, synaptic partners, or projection targets, all of which are critical for predicting how receptor activation will alter circuit function.

The implications for drug development are substantial. Cell-type-specific receptor maps enable predictions about which neural populations will be directly affected by specific drugs, which can guide the interpretation of behavioral effects and the design of more selective compounds. For example, the high Htr2c expression in BLA excitatory neurons suggests that 5-HT2A agonists with lower 5-HT2C activity may produce less amygdala-dependent anxiety than non-selective compounds. The preferential expression of alpha-1 receptors in interneurons suggests that prazosin's effects may be mediated by disinhibition rather than direct suppression of principal neurons. The high Htr2a expression in Lamp5 interneurons suggests that psychedelics may modulate disinhibitory circuits that gate sensory information and emotional salience. Each of these predictions can be tested experimentally using cell-type-specific manipulations, and confirmed through measurements of drug effects on defined cell populations.

Future directions for this work include extending the analysis to other anxiety-relevant brain regions such as the ventral hippocampus, bed nucleus of the stria terminalis, and periaqueductal gray. Integrating receptor expression data with circuit connectivity information from the Allen Brain Connectivity Atlas would enable prediction of how receptor activation propagates through anatomically defined pathways. Comparing receptor profiles between mouse and human using human postmortem or surgical tissue data would identify conserved versus species-specific patterns. Most importantly, functional validation using cell-type-specific receptor knockout or optogenetic/chemogenetic modulation during psychedelic administration or fear conditioning would test whether high receptor expression predicts functional importance. The present dataset provides a comprehensive molecular foundation for these future mechanistic and translational investigations into the cellular basis of monoaminergic modulation of fear and anxiety circuits.

Supplementary Figures

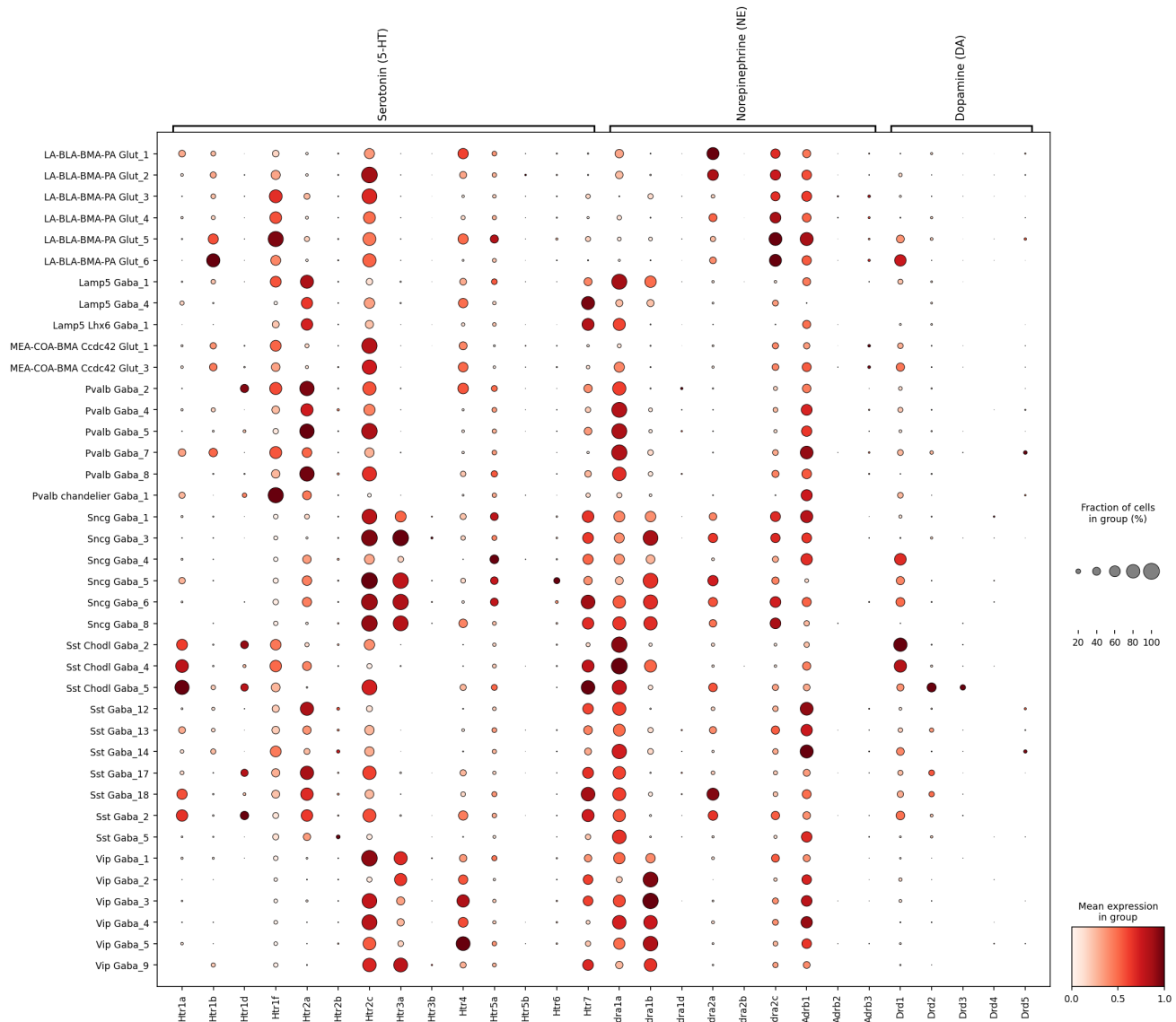


Figure S1. Fine-grained BLA receptor expression at supertype resolution (10x scRNA-seq). Dot plot showing 28 receptor genes across BLA supertypes with ≥ 50 cells, representing 68 distinct cell populations (28,809 cells). This higher-resolution view reveals subtype-specific expression patterns masked at the subclass level.

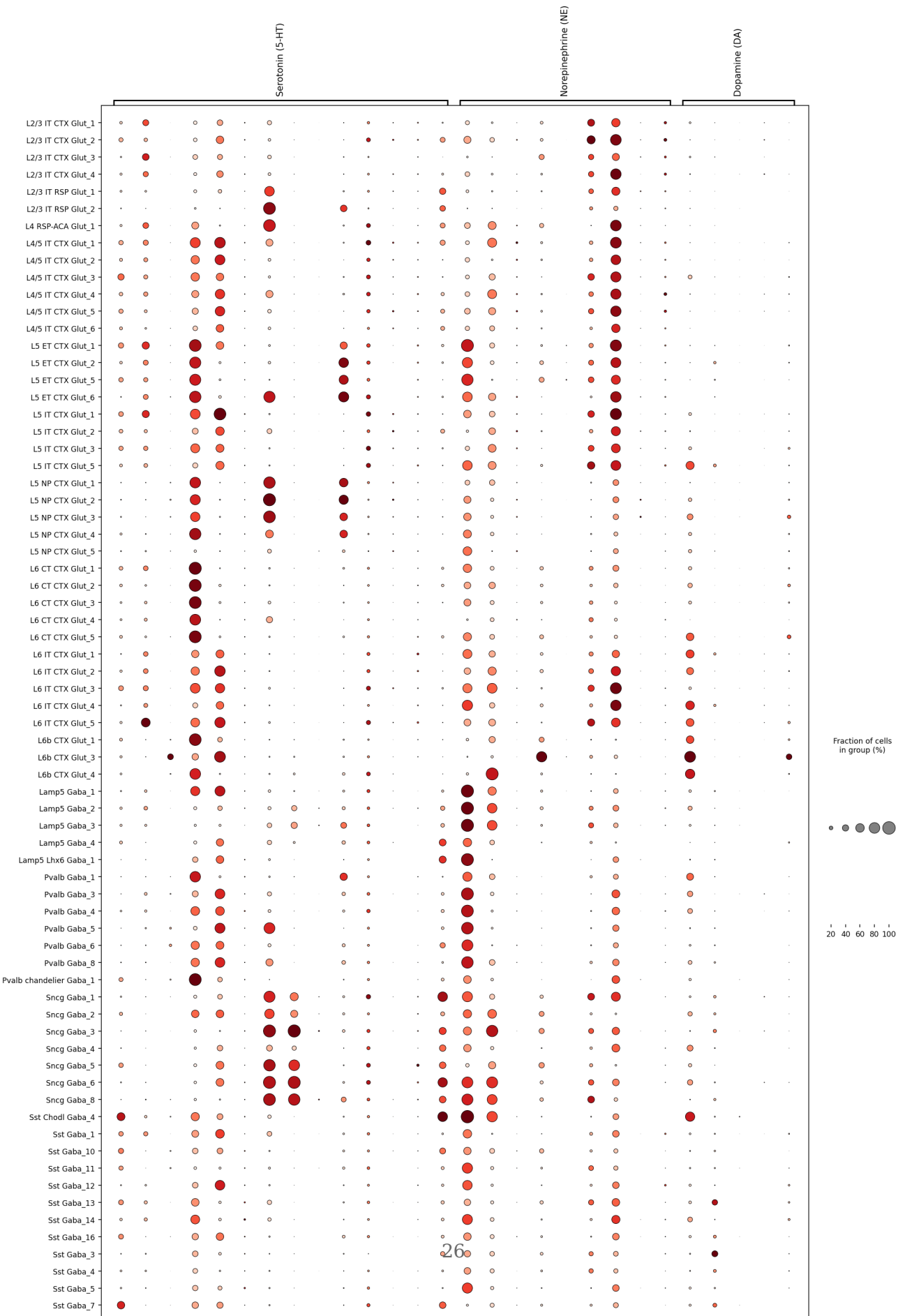


Figure S2. Fine-grained mPFC receptor expression at supertype resolution (10x scRNA-seq). Dot plot showing 28 receptor genes across mPFC supertypes with ≥ 50 cells, representing 101 distinct cell populations from 165,539 cells.

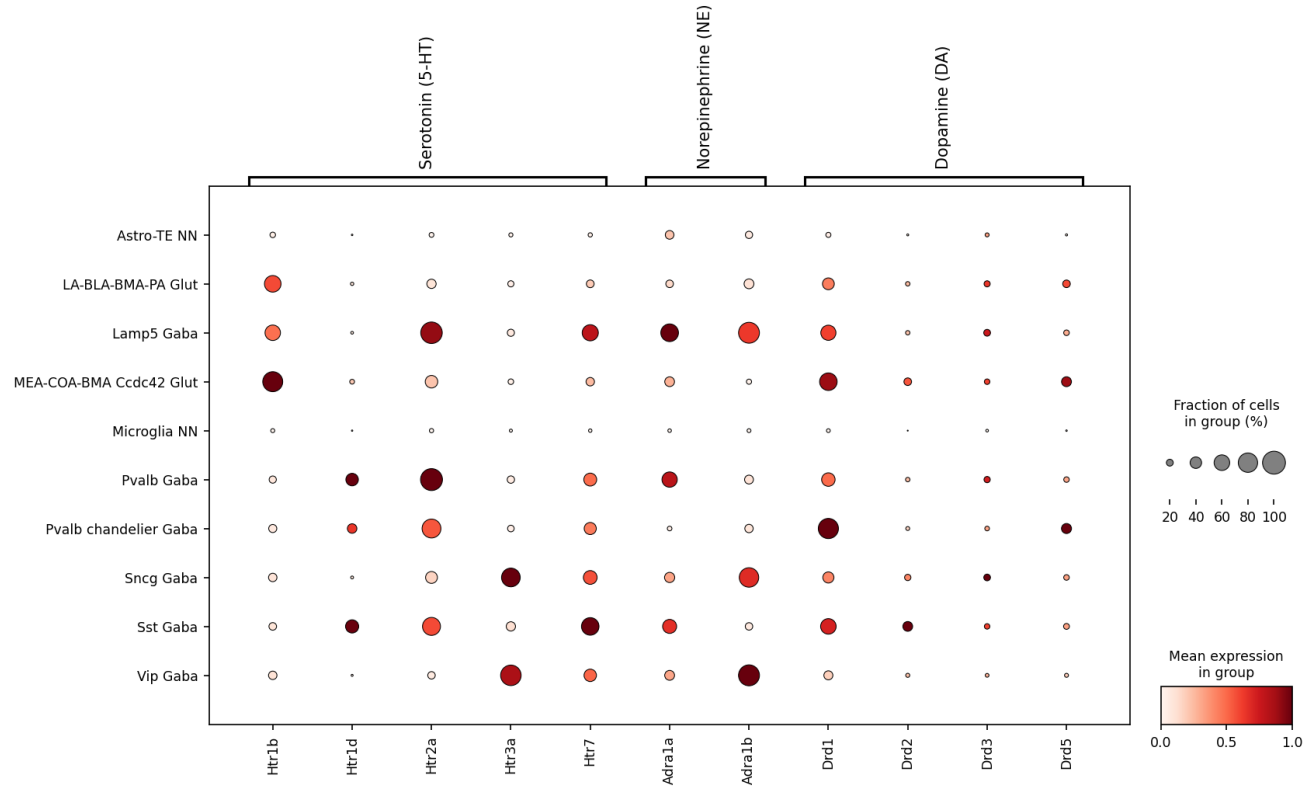


Figure S3. BLA MERFISH receptor expression at subclass resolution. Subclass-level dot plot (10 cell types, 11 genes, 8,238 cells). MERFISH spatial resolution confirms that all cell types are localized within BLA, providing ground truth for cell-type-specific receptor expression.

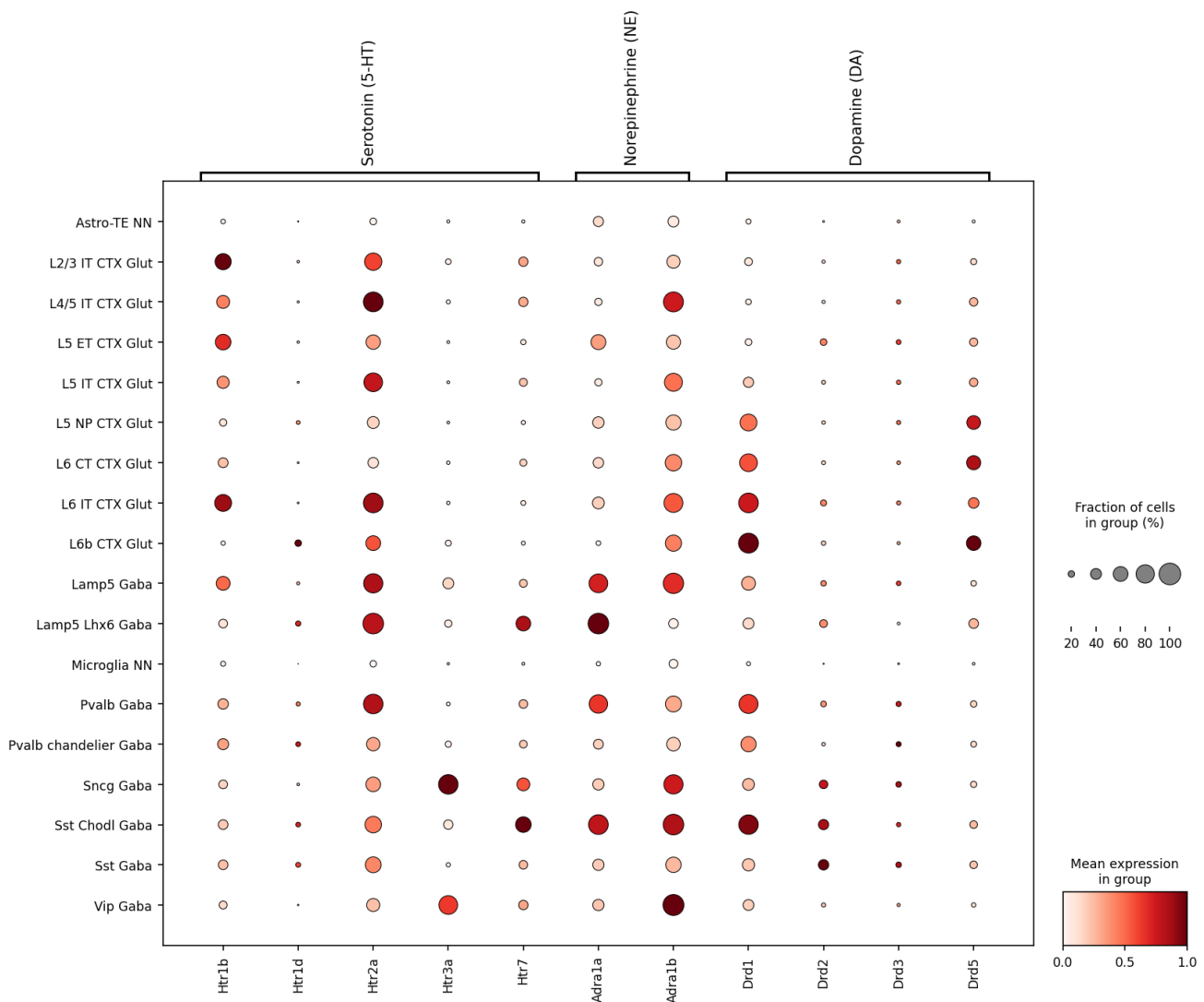


Figure S4. mPFC MERFISH receptor expression at subclass resolution. Subclass-level dot plot (18 cell types, 11 genes, 64,474 cells). Spatially validated mPFC cell types demonstrate area-specific receptor expression.

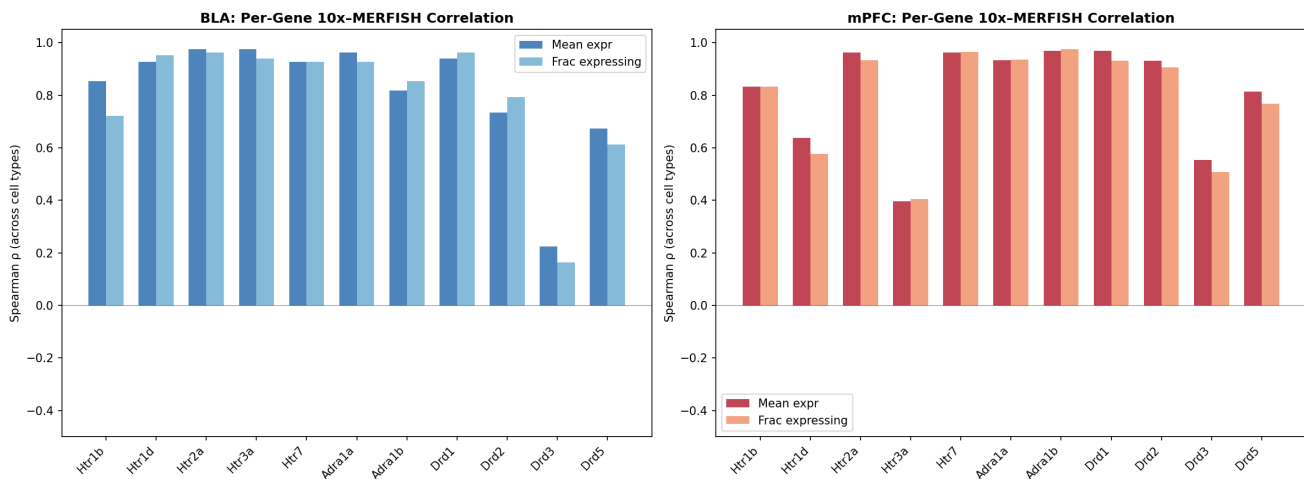


Figure S5. Per-gene cross-modality correlations. Bar plots showing Spearman rho between 10x and MERFISH for each of 11 shared receptor genes, across cell types in BLA and mPFC. High per-gene correlations ($\rho > 0.7$) indicate robust cell-type specificity.

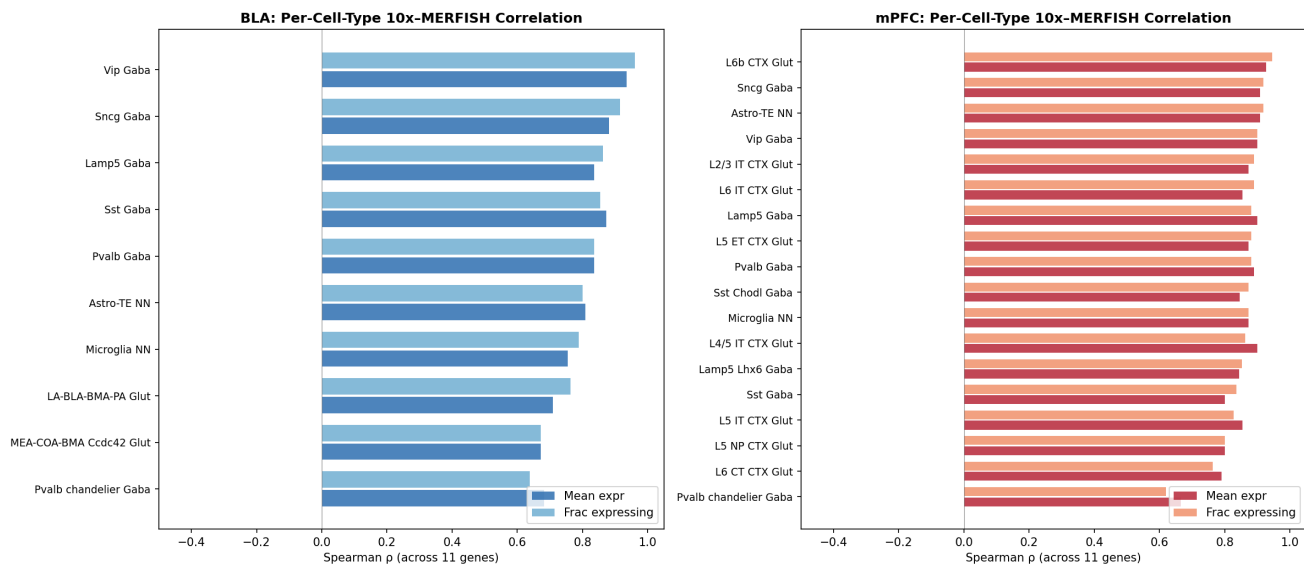


Figure S5b. Per-cell-type cross-modality correlations. Bar plots showing per-cell-type correlations across the 11 genes for BLA and mPFC. High per-cell-type correlations indicate reproducible receptor profiles.

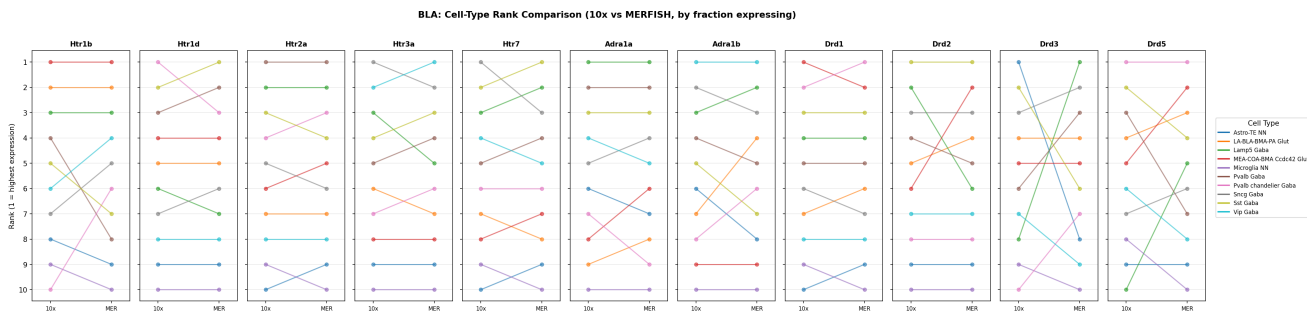


Figure S6a. Rank comparison for BLA (10x vs MERFISH). Cell types are ranked for each gene in each modality. Visual comparison of rank agreement between platforms.

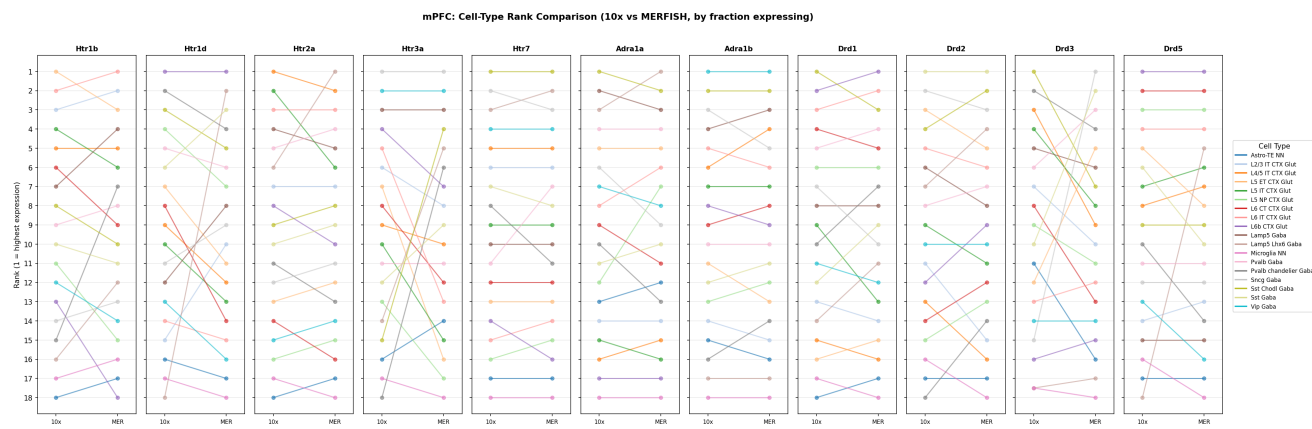


Figure S6b. Rank comparison for mPFC (10x vs MERFISH). Corresponding rank comparison for mPFC cell types.

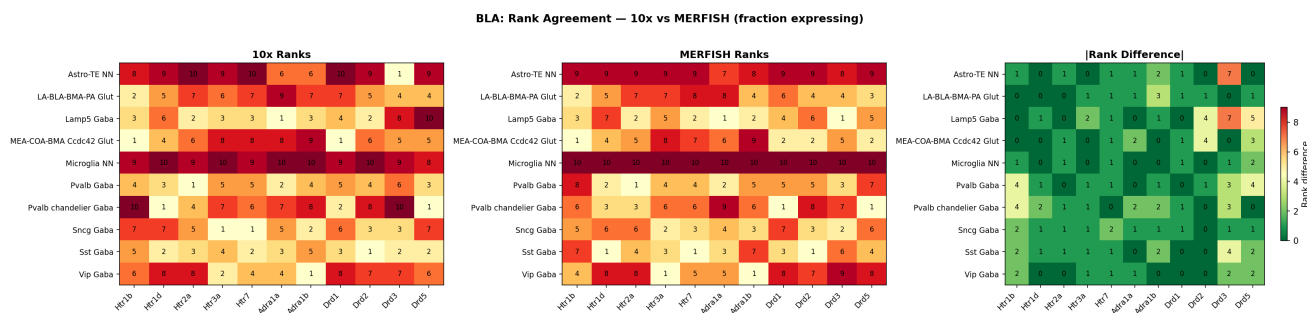


Figure S6c. Rank agreement heatmap for BLA. Absolute rank differences between 10x and MERFISH. Green = perfect agreement, red = maximal disagreement.

mPFC: Rank Agreement — 10x vs MERFISH (fraction expressing)

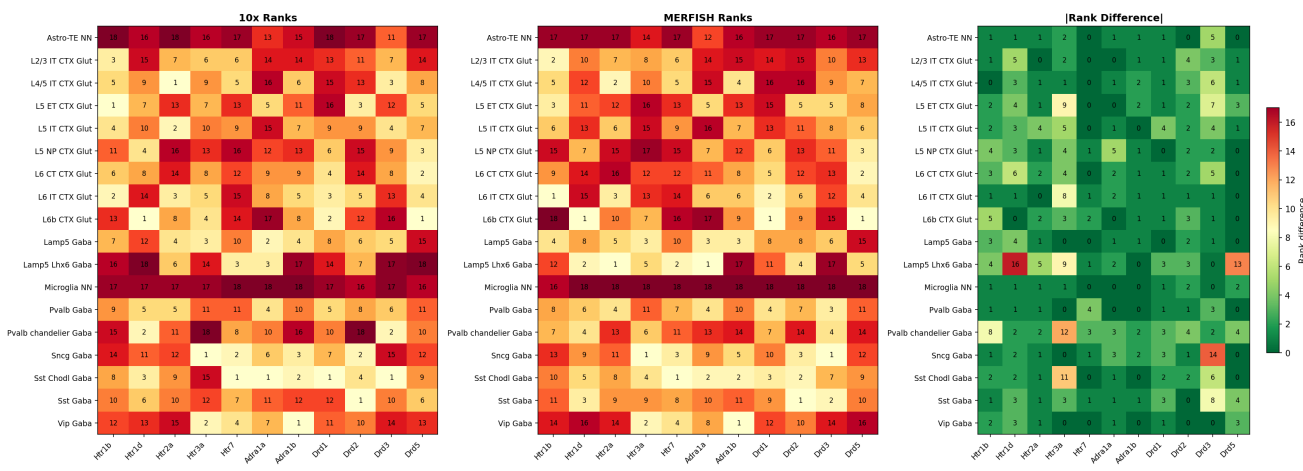


Figure S6d. Rank agreement heatmap for mPFC. Corresponding rank agreement for mPFC across 18 shared cell types.

MERFISH: BLA vs mPFC Cross-Region Correlation

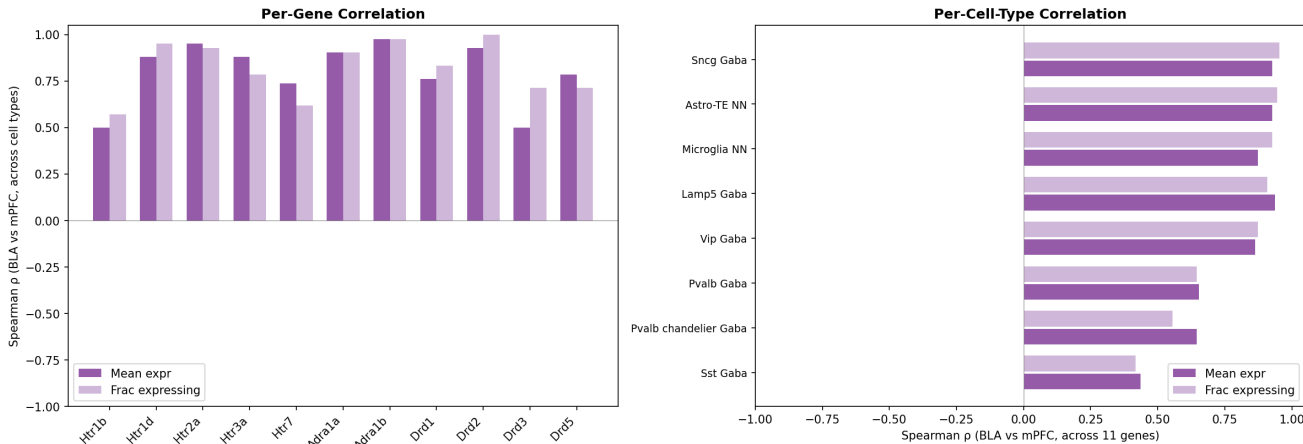


Figure S7a. Per-gene cross-region correlations (MERFISH). Spearman correlations between BLA and mPFC expression across shared interneuron/glial types for 11 genes.

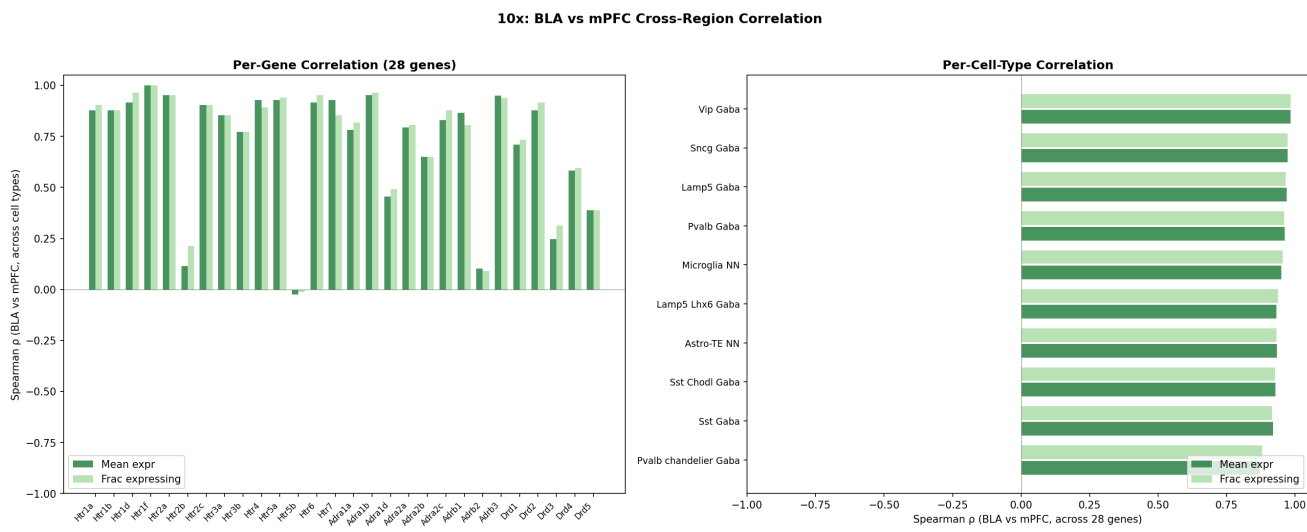


Figure S7b. Per-gene cross-region correlations (10x). Spearman correlations for all 28 genes across 10 shared types.

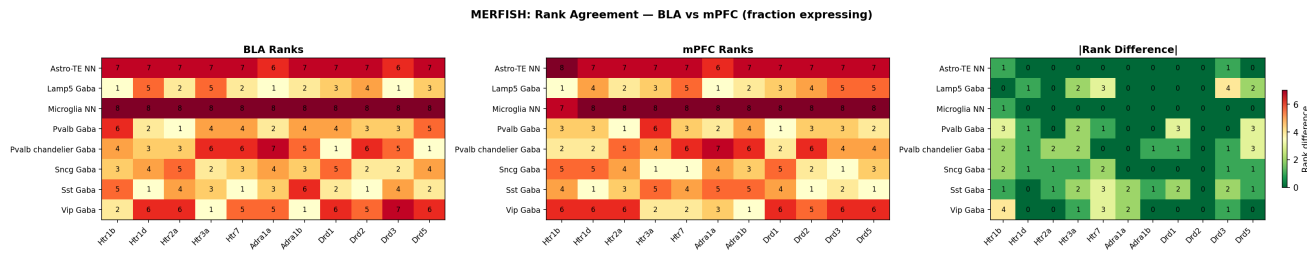


Figure S7c. Cross-region rank agreement (MERFISH). Rank agreement heatmaps comparing BLA versus mPFC cell-type rankings for each gene.

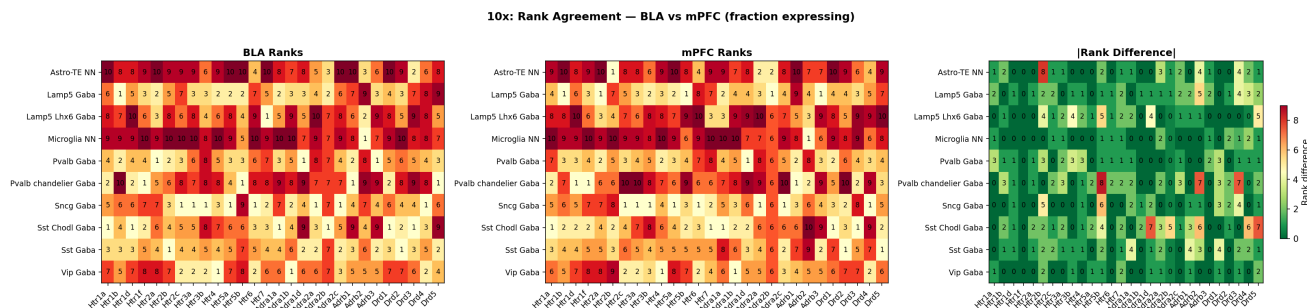


Figure S7d. Cross-region rank agreement (10x). Rank agreement for all 28 genes across 10 shared cell types.

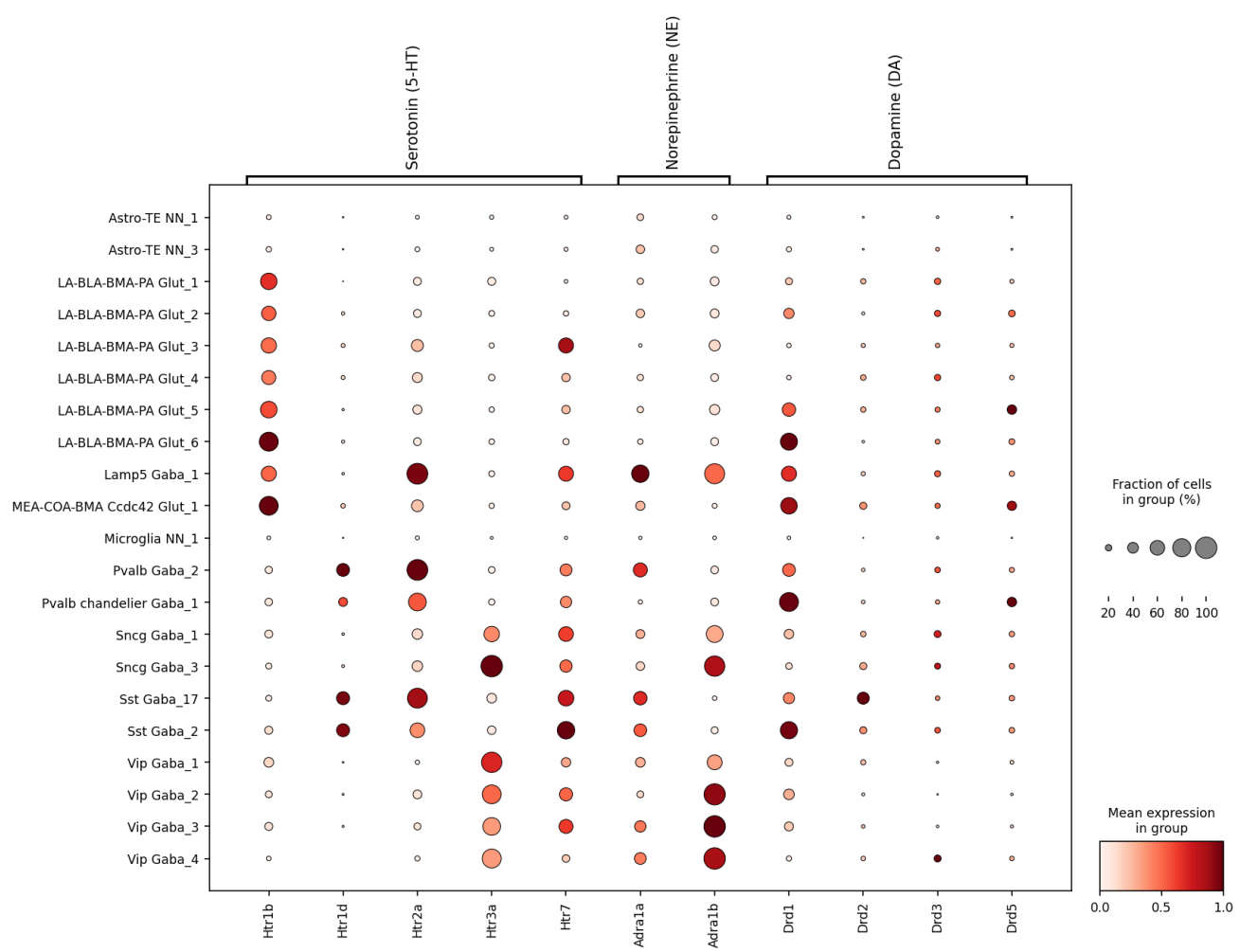


Figure S8. BLA MERFISH receptor expression at supertype resolution. Fine-grained dot plot showing receptor expression across BLA supertypes in the MERFISH dataset.



Figure S9. mPFC MERFISH receptor expression at supertype resolution. Fine-grained dot plot showing receptor expression across mPFC supertypes in the MERFISH dataset.

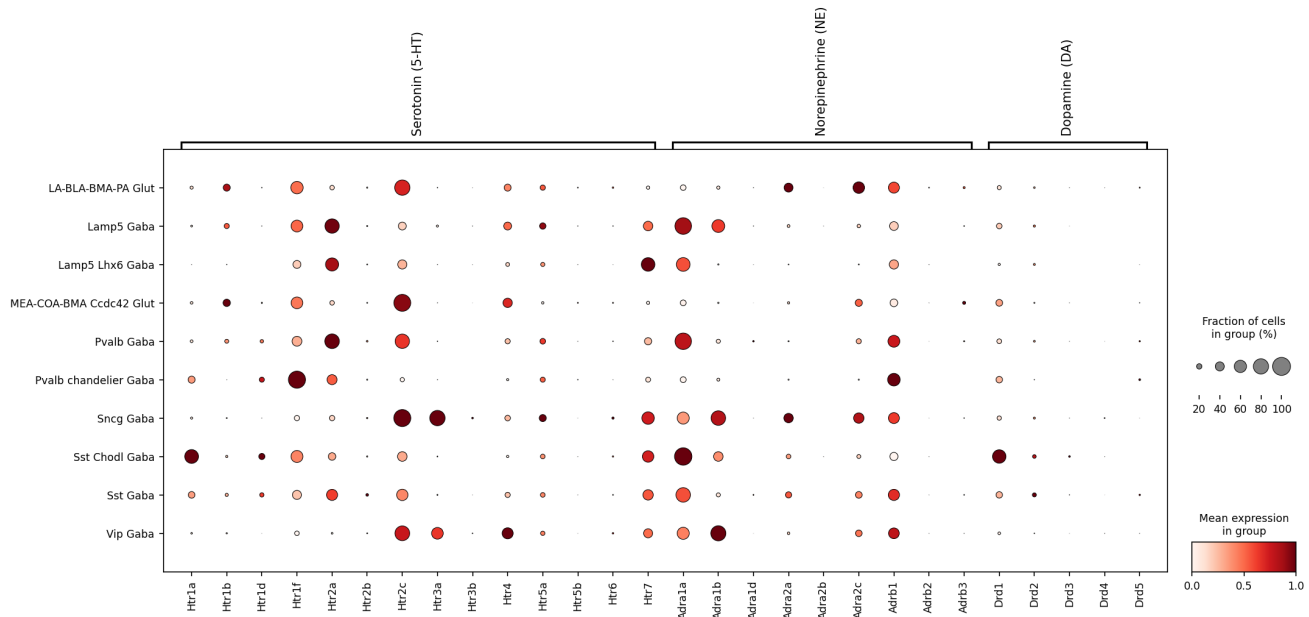


Figure S10. BLA 10x receptor expression at subclass resolution (neuronal only). Dot plot showing 28 receptor genes across BLA neuronal subclasses without glia.

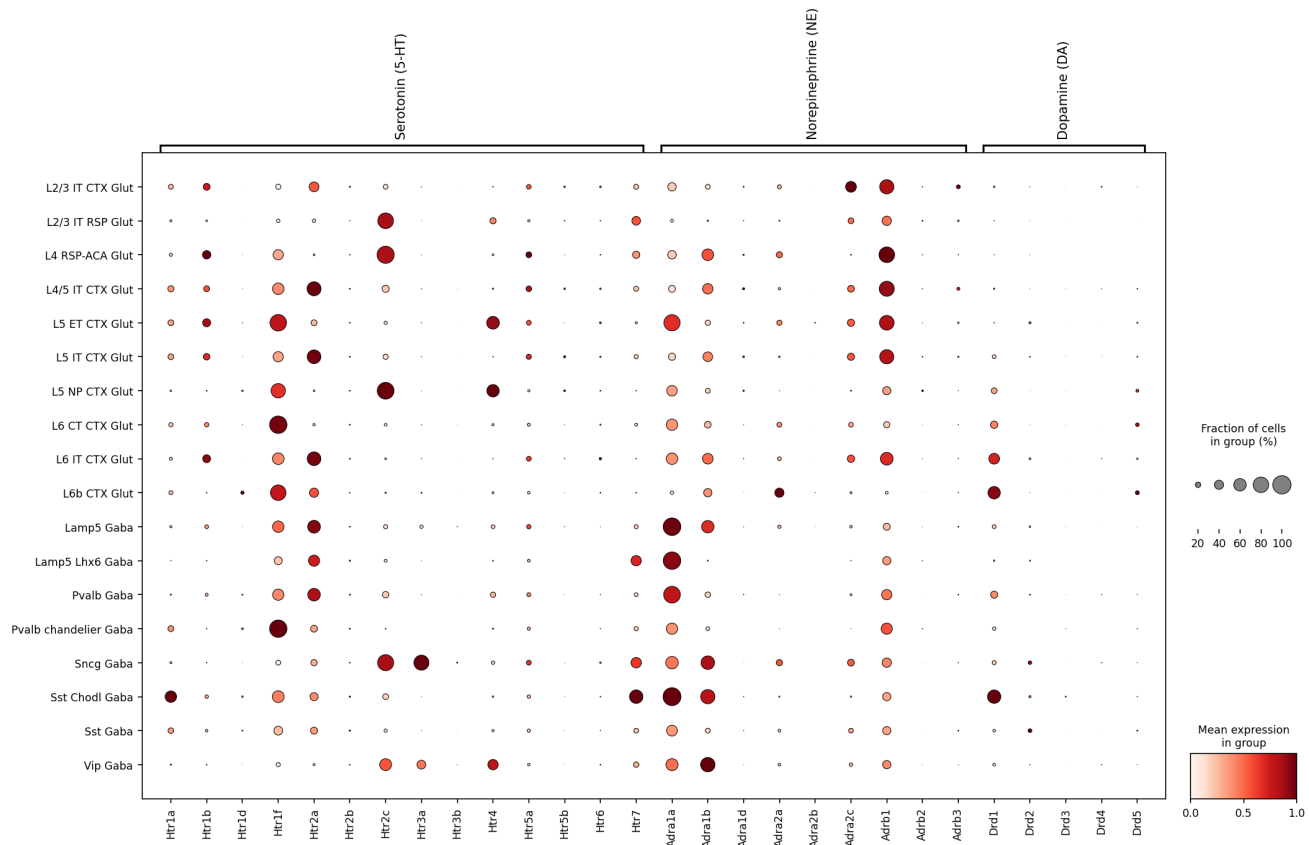


Figure S11. mPFC 10x receptor expression at subclass resolution (neuronal only). Dot plot showing 28 receptor genes across mPFC neuronal subclasses without glia.